Overcoming the Blood-Brain-Tumour Barrier Using Superparamagnetic Iron Oxide Nanoparticles *in Vitro*

Master Thesis

Frederik Hegner Odgaard

9^{th}-10^{th} Semester

Department of Health Science and Technology, Aalborg University
Medicine with Industrial Specialization, Biomedicine

Medicine with Industrial Specialization, Biomedicine
Aalborg University
http://www.aau.dk

AALBORG UNIVERSITY
STUDENT REPORT

Title:
Overcoming the Blood-Brain-Tumour Barrier Using Superparamagnetic Iron Oxide Nanoparticles *in Vitro*

Project Period:
September 1st 2023 to August 14th 2024

Project Group: 9021

Participant(s):

Frederik Hegner Odgaard;
study no. 20185799

Supervisor:
Louiza Bohn Thomsen

Page Numbers: 50

Date of Completion:
August 14, 2024

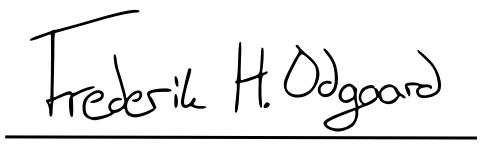

Abstract

Introduction

Glioblastoma multiforme (GBM) is the highest killing brain tumour with a prognosis of only 12 months. The blood-brain barrier (BBB) poses an enormous obstacle for most drug delivery to the brain. In the presence of a brain tumour, the surrounding vasculature becomes slightly altered and leaky forming the blood-brain-tumour barrier (BBTB). This compromised barrier can potentially be a gateway for drug delivery. Magnetic nanoparticles (MNPs) are easily modifiable and it is possible to direct to a desired treatment site by en external magnetic force. The aim of this study is to evaluate the transport of MNPs over the BBTB.

Methods

An *in vitro* BBTB was constructed using a co-culture of either porcine brain endothelial cells (PBECs) or human brain microvasculature endothelial cells (HBMECs) with T10 GBM cells. U87 GBM cells were used as a control for T10 cells, and a mono-culture BBB model was used as a control for the BBTB setup. The treatment consisted of either MNPs combined with the subjection of an external magnetic field, MNPs without magnetic subjection and a control with no treatment. Fluorescent microscopy and Perl's prussian blue analysis was used to visualise and quantify the passage of MNPs into and through the endothelial cells. Additionally transendothelial electrical resistance (TEER) measurements were made to evaluate the integrity of the BBB.

Results

FluidMAG-ARA nanoparticles did not exert any cytotoxic effect towards PBECs or HBMECs ($p>0.05$), but did seem to be somewhat toxic for U87 cells ($p<0.05$). Neither did the MNPs result in any significant decrease in TEER for any of the BBB or BBTB models ($p>0.05$). Immunocytochemistry showed that no MNPs were internalised by the endothelial cells. Based on analysis of the medium from the bottom wells of all treated BBB and BBTB model, using either fluorescent microscopy or Prel's prussian blue method, none of the MNPs did pass any of the barriers. Finally, is was evident that thee MNPs were able to pass through the membrane of inserts with no cells. Furthermore, showing a difference between the concentration of MNPs transported through an insert with cells compared with one without cells ($P<0.0001$).

Conclusion

An *in vitro* BBTB model was established with T10 or U87 cells. Contrary to the expectations, MNPs did not cross the *in vitro* BBTB or BBB model at any concentration or subjected by an external magnetic field. However the MNPs did not exert any cytotoxic effect to the endothelial cells. Therefore, the potential of using these MNPs for targeted drug delivery remains.

Acknowledgement

I would like to give a special thanks to my supervisor Louiza Bohn Thomsen for her kindness and for welcoming me in to the medical microbiology and immunology group. I am grateful for all her help and optimistic support when things did not go as planned. She has taught me a great deal of what it means to be an excellent researcher.

I would like to thank everyone in the MMI group for good fellowship and usefully feedback during group meetings.

Likewise I wish to thank my fellow master students for always being helpful and supportive. A special thanks to Elaxmi Sathiylingam for her help and support throughout the project period.

Contents

List of Abbreviations

- AMT - Adsorptive medidated transport
- ANOVA - Analysis of variance
- ATP - Adenosine triphosphate
- BBB - Blood-brain barrier
- BBTB - Blood-brain-tumour barrier
- BECs - Brain endothelial cells
- bFGF - Basic fibroblast growth factor
- BM - Basement membrane
- BSA - Bovine serum albumin
- CNS - Central nervous system
- cAMP - Cyclic adenosine monophosphate
- DAPI - 4’,6-diamidino-2-phenylindole
- DLS - Dynamic light scattering
- DMEM - Dulbecco’s modified eagle medium
- DMEM-F12 - Dulbecco’s modified eagle medium containing nutrient mixture F12
- DMSO - Dimethyl sulfoxide
- DNA - Deoxyribonucleic acid
- EDC - 1-ethyl-3-(3-dimethylaminopropyl) carboodiimide
- EGF - Epidermal growth factor
- GBM - Glioblastoma multiform
- HBMEC - Human brain microvascular endothelial cells
- HC - Hydrocortisone
- HCL - Hydrochloric acid
- ITS - Insulin-transferrin-selenium
- JAM - Junctional adhesion molecules
- IDH - Isocitrate dehydrogenase
- MES - 2-(N-Morpholino)ethanesulfonic acid

- MRI - Magnetic resonance imaging
- NVU - Neurovascular unit
- PFA - Paraformaldehyde
- PBEC - Porcine brain endothelial cells
- PBS - Phosphate buffered saline
- PDGFR - Platelet-derived growth factor
- P-gp - P-glycoprotein
- RMT - Receptor mediated transcytosis
- RRT-qPCR - Reverse transcription-quantitative polymerase chain reaction
- SD - Standard deviation
- TEER - Transendothelial electrical resistance
- TfR - Transferrin receptor
- TME - Tumour microenvironment
- TP53 - Tumour protein 53
- VEGF - Vascular endothelial growth factor
- ZO-1 - Zonula occludens-1

Introduction

1.1 Glioblastoma multiforme

Glioblastoma multiforme (GBM) is the most commonly occurring and aggressive malignant brain tumour (Price et al., 2024). In Denmark, the incidence rate is 6.3/100,000 for men and 3.9 for females and a median age of 66 years (Hansen et al., 2018) and has a poor prognosis with a median survival time of 12 months with a 5% chance of 5-year survival (Gallego, 2015). The etiology of GBM is in most cases unknown. The only well-known non-genetic risk factor for GBM is high doses of ionised radiation. (Kanderi & Gupta, 2022) GBM arises from the glial cells and occurs sporadically and shows no sign of genetic predisposition (Krex et al., 2007), except in cases of Turcot syndrome (Hamilton et al., 1995) and Li-Fraumeni syndrome (Sloan et al., 2020). The World Health Organisation (WHO) made an updated classification of GBM in 2021 reserving the term for isocitrate dehydrogenase (IDH) wildtype grade 4 astrocytomas only (Louis et al., 2021). GBM is highly heterogeneous and remains difficult to treat due to its treatment resistance and high recurrence rate. Glioblastoma stem-like cells (GSCs) are a main cause for GBM tumour infiltration presenting the cells with self-renewing and differentiation properties (Lathia et al., 2015). GBM is difficult to treat because it retains multiple cellular and metabolic mechanisms to help grow and spread (Esemen et al., 2022).

1.1.1 GBM microenvironment

Aggressive tumours such as GBM are characterised by certain tumourigenic properties like cell proliferation, migration and invasion of surrounding tissue as well as resistance to treatment. These traits are achieved through modifying their microenvironment (Mbeunkui & Johann, 2009). The GBM tumour microenvironment (TME) is a complex and dynamic system that can be influenced by several factors like cell composition, cell-to-cell contact, cellular metabolites as well as other chemical factors like pH and oxygen levels (Sharma et al., 2023). GBM cells constantly work to reprogram the TME control to benefit their survival thereby making it highly heterogeneous and resistant to treatment. The communication between the tumour and the surrounding cells is done through cytokines, chemokines, matrix remodelling enzymes and growth factors (Erices et al., 2023; Sharma et al., 2023).

The TME is comprised of endothelial cells, astrocytes, oligodendrocytes, immune cells such as microglia, tumour-infiltrating circular immune cells and non-cellular components like apocrine and paracrine signalling molecules, exosomes, and extracellular matrix components (Martinez-Lage et al., 2019; Sharma et al., 2023). GBM tumour cells produce a variety of growth factors to support the tumour, including vascular endothelial growth factor (VEGF) which is a strong angiogenic factor supporting the creation of new blood

vessels. VEGF acts by downregulating tight junctions leading to a leaky blood-brain barrier (BBB) with higher permeability and more fenestration in the brain endothelial cells (BECs) (Erices et al., 2023). The rapid formation of new blood vessels leads to the fast development of the tumour, but also leads to a more permeable BBB due to the abnormality of the newly formed vessels. This can cause large molecules to passively diffuse to the extracellular fluid like water causing edema. (Erices et al., 2023; Tripathy et al., 2024) Although the newly formed vessels are more permeable, this does not mean it is easier to treat these tumours with therapeutics. This is because the new vessels contain a higher number of efflux transporter proteins such as P-glycoprotein (P-gp) and multidrug resistance protein (MRP) that inhibit the transport of drugs across the BBB by constantly pumping them out of the endothelial cells. (Tripathy et al., 2024)

1.2 Treatment of GBM

The complexity and heterogeneity of the TME as described above make GBM extremely challenging to treat and highly recurrent. This means that while parts of the tumour cells might react to one type of treatment, others will resist it and cause the tumour to survive (Anjum et al., 2017). The common treatment protocol for GBM patients consists of surgical resection, radiation therapy and chemotherapy with temozolomide. These treatments may be combined depending on the stage, location and size of these tumours (Anjum et al., 2017). Current treatment options for GBM are insufficient and they do not provide any long term treatment for the patients (Erices et al., 2023). This low efficacy of treatment is due to the aggressive tumour infiltration in the surrounding tissue making total surgical resection very difficult and GBM recurrence is inevitable (Erices et al., 2023). Other challenges that make the current treatment options insufficient include; tumour heterogeneity, glioma stem cells, drug efflux pumps, DNA repair mechanisms and the blood-brain barrier (Angom et al., 2023). Although there is a vast variety of challenges, this also means a lot of opportunities for therapy development (Angom et al., 2023).

1.3 The blood-brain barrier

The neurovascular unit (NVU) is the functional structure of the brain and is comprised of neurons, glial cells, vascular cells and their basal lamina (Arvanitis et al., 2020; Kugler et al., 2021) (see figure 1.1 a.). The blood-brain barrier (BBB) is part of the NVU and is a naturally occurring semi-permeable barrier in the central nervous system (CNS) formed by the non-fenestrated brain endothelial cells (BECs) in the capillaries (Soto-Rojas et al., 2021). These cells are tightly connected by tight junctions and adherence junctions which make up this barrier. Tight junctions consist of transmembrane proteins such as claudin, occludin and junctional adhesion molecules (JAMs) as well as cytoplasmic plaque proteins like Zonula occludens (ZO)-1, ZO-2 and ZO-3 (W.-Y. Liu et al., 2012). These proteins create a highly selective barrier controlling what passes through, thereby protecting the brain tissue from harm (W.-Y. Liu et al., 2012). Tight junctions are dynamic structures and are therefore able to change their permeability as a reaction to certain signals and conditions such as

inflammation and disease (Luissint et al., 2012). Claudin and occludin are both integrated membrane proteins consisting of two extracellular domains, four transmembrane domains and three cytoplasmic domains. Caludin 5 is expressed in the endothelial cells in most of the brain and is a hallmark of the BBB playing an essential role in CNS angiogenisis. Together these proteins ensure a tight barrier (Jiao et al., 2011; W.-Y. Liu et al., 2012). The ZO proteins belong to the membrane-associated guanylate kinases with an N-terminus containing three PDK domains. The multiple binding sites of the ZO proteins allow them to bind to each other or function as scaffold proteins connecting the actin cytoskeletotn and the transmembrane proteins like occludin and claudin 5 (Zheng et al., 2023). The tight junctions between the BECs make up a tight paracellular connection with a high transendothelial electrical resistance (TEER) (M. S. Thomsen et al., 2021). The BECs are supported by pericytes embedded in the basement membrane as well as astrocyte endfeet that help regulate the barrier. The components of the NVU serve to maintain proper brain function, regulate blood flow and sustain the BBB (Fu, 2018). The BBB keeps the brain in homeostasis through a tight restriction and control of what blood-borne substances pass through the barrier, thereby preventing any toxins or pathogens from entering and causing damage or inflammation to the brain tissue (Abbott et al., 2010; Fu, 2018) (see figure 1.1 b.).

The barrier formed by the BECs only allows passive diffusion of lipid-soluble drugs at a molecular weight of less than 400-600Da. BECs are non-fenestrated which limits the free diffusion and rapid exchange of molecules between the brain tissue and the blood (Wu et al., 2023). BECs also contain a higher amount of mitochondria than peripheral endothelial cells, implying higher energy demands of the BECs due to the specialised functions of the BBB (Oldendorf et al., 1977). The morphology of the BECs makes transport difficult. The cells present with net negative surface charge, only allowing a minimum of negatively charged molecules to pass. BECs are also equipped with special transporters to control the inflow and outflow of specific substrates (Wu et al., 2023) (see section 1.5).

Other important components that support and strengthen the BBB are astrocytes and pericytes. Astrocytes form an important connection between the vessel and the neural circuit. Astrocytes stretch out their endfeet whereby they help clear waste, control brain blood flow, and regulate vascular function and ion homeostasis (Abbott et al., 2006; Petzold & Murthy, 2011; Verkhratsky & Nedergaard, 2018). Pericytes are located along the walls of the capillary blood vessels and they are embedded in the basement membrane. Pericytes send important signalling factors to the BECs to help determine the number of tight junctions. (Fu, 2018; Gawdi & Emmady, 2020) However, the strength of the BBB complicates the pharmacotherapy for CNS disorders and tumours as most of the drugs capable of treating these diseases are incapable of crossing the BBB. This can lead to insufficient therapeutic efficacy and a higher risk of side effects due to the accumulation of the drug in other tissues. (Fu, 2018)

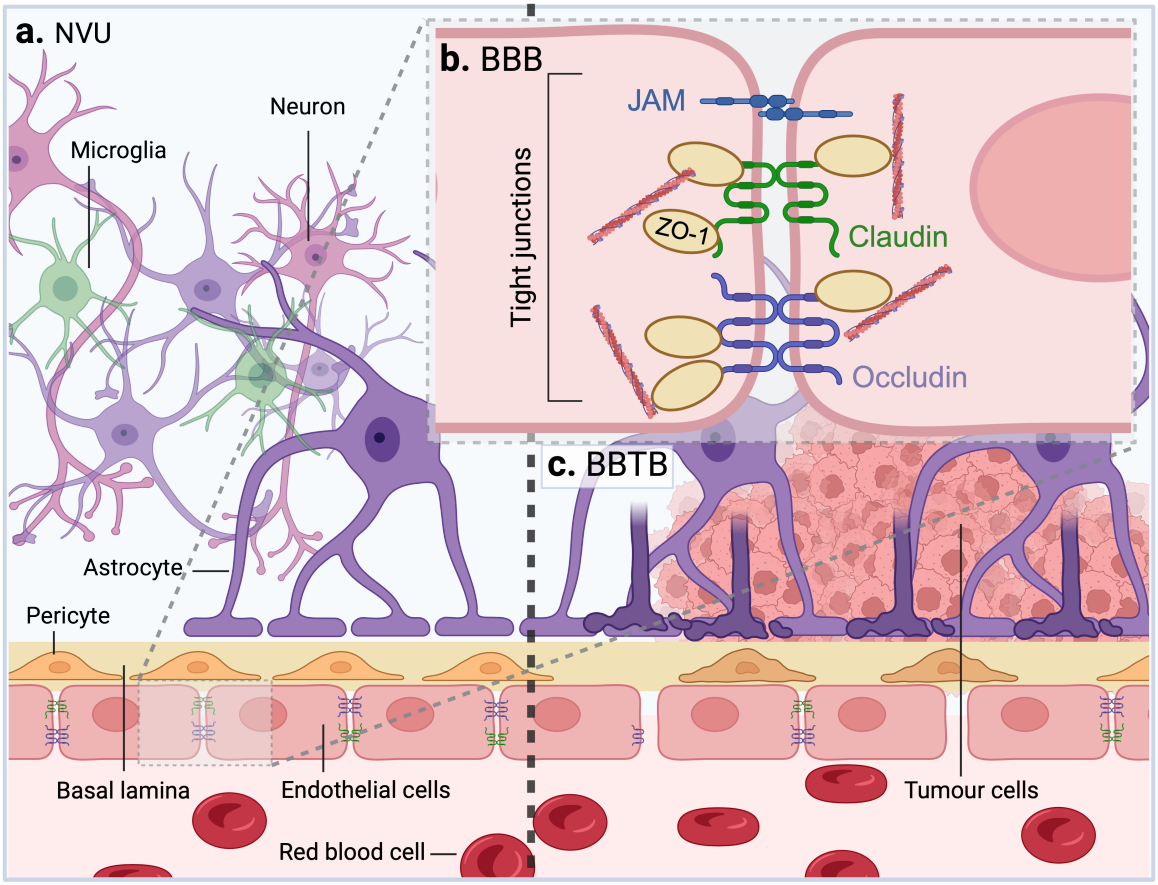

Figure 1.1: The neurovascular unit including the BBB and BBTB. a. The NVU is the functional structure of the brain and is composed of neurons, glial cells, vascular cells and their basal lamina. **b.** The BBB consists mainly of the endothelial cells and the tight junction proteins ZO-1, claudin-5 and JAMs. The BBB help protect the brain by creating a barrier between the blood and the brain. This barrier is supported by the astrocytes and pericytes. **c.** BBTB is illustrated by loss of astrocytic endfeet and a compromised integrity with increased and variable permeability. This figure was inspired by (Arvanitis et al., 2020) and made in BioRender.com.

1.4 The blood-brain-tumour barrier

In the presence of a tumour, the BBB tends to be slightly altered and is often refereed to as the blood-brain-tumour barrier (BBTB) (see figure 1.1 c.). The nature of the cancer cells forces them to create the optimal environment for survival no matter the consequences for the surrounding tissue (Arvanitis et al., 2020). Tumourigenesis demands increased nutrients and oxygen which induces angiogenesis by stimulating the expression of proangiogenic factors such as VEGF, epidermal growth factor (EGF) and platelet-derived growth factor (PDGFR). Due to the deregulation of angiogenic factors and hypoxia, the tumour microvasculature is often abnormal and functionally immature of varying size and permeability. (Ahir et al., 2020)

.

Generally, the BBTB is characterised by having a thicker basal membrane, loss of astrocytic endfeet and a compromised integrity with increased and variable permeability (Arvanitis

et al., 2020). Moreover, irregular, abnormal and leaky vasculature is a common problem in the BBTB (Rathi et al., 2022). Due to the compromised integrity of the barrier, it is less selective, thereby allowing larger molecules and a broader range of substrates to pass through (Rathi et al., 2022). Studies have found that therapeutics accumulate at a higher concentration in brain tumours than in normal brain tissue, indicating easier drug delivery to the tumour (Chen et al., 2022; Kong et al., 2012; Stylianopoulos et al., 2018). However, this is not always the case due to the upregulation of efflux transporter proteins in the newly formed BECs (Wilhelm et al., 2016).

1.5 Transport across the BBB/BBTB

The brain is the most energy-consuming organ in the body and needs a lot of nutrients and regulatory molecules (Fu, 2018). For this reason, a normal part of the BBB function involves a variety of transport mechanisms through the barrier, these transport mechanisms are both passive and active (see fig 1.2) (Pulgar, 2019). The BECs making up the BBB are different from those in the peripheral microvessels in that they have far tighter junctions between them and much less fenestration (Fu, 2018). The tightness makes transport through the barrier much more difficult, and more dependent on lipid solubility, molecular size, electrical charge and binding to different surface transporters and receptors (Fu, 2018). Compared to the peripheral tissue, the tight junctions in the BECs tightly restrict the paracellular transport of hydrophilic molecules (Fu, 2018; Wu et al., 2023).

Small hydrophobic molecules such as O^2 and CO^2 can diffuse freely across the membrane (Abbott et al., 2010). Transport across the BBB may also be facilitated by certain transport proteins, such as ion transporters, specific transporters and energy-dependent pumps(Fu, 2018). Other solutes, such as glucose and amino acids, that are essential for the brain, pass the BBB using these transport proteins (Fu, 2018). The solutes bind to the transporter and initiate a conformational change in the protein leading to moving the substrate with the concentration gradient(Fu, 2018). Some of these transporters can transport solutes against the concentration gradient at the cost of ATP (Fu, 2018).

Receptor-mediated transcytosis is the process where a certain macromolecule, such as insulin, binds to its corresponding receptor (Abbott et al., 2010). The ligand and the receptor are then enveloped in a vesicle by endocytosis and transported through the cytoplasm to the abluminal side of the BECs to be exocytosed and released into the brain (Fu, 2018; Lee & Jayant, 2019).

Positively charged proteins can, by interacting with the negatively charged membrane, initiate adsorptive-mediated transcytosis or pinocytosis, allowing for the given protein to bind to the luminal surface of the BECs and later undergo exocytosis at the abluminal surface, thereby releasing the protein to the brain (Fu, 2018).

One of the most challenging transport mechanisms when it comes to drug delivery to the

brain is the efflux pumps. The BBB is equipped with other proteins like P-glycoprotein (P-gp) and multidrug resistance protein (MRP) that act as efflux proteins (Busquets et al., 2015; Löscher & Potschka, 2005). These pumps are part of the ATP-binding cassette gene family and are responsible for expelling both endogenous and exogenous compounds, like drugs from the BECs to the blood. They work by consuming ATP to transport different lipid-soluble molecules, that otherwise would have been able to cross the membrane, out of the cell (Busquets et al., 2015; Löscher & Potschka, 2005).

Recent studies have proved advances in the transport of magnetic particles through the BBB by external exposure to a magnetic field. This suggests a modified transport path which is highly controllable and especially useful in drug delivery across the BBB (Chertok et al., 2008; Kong et al., 2012; L. B. Thomsen et al., 2013).

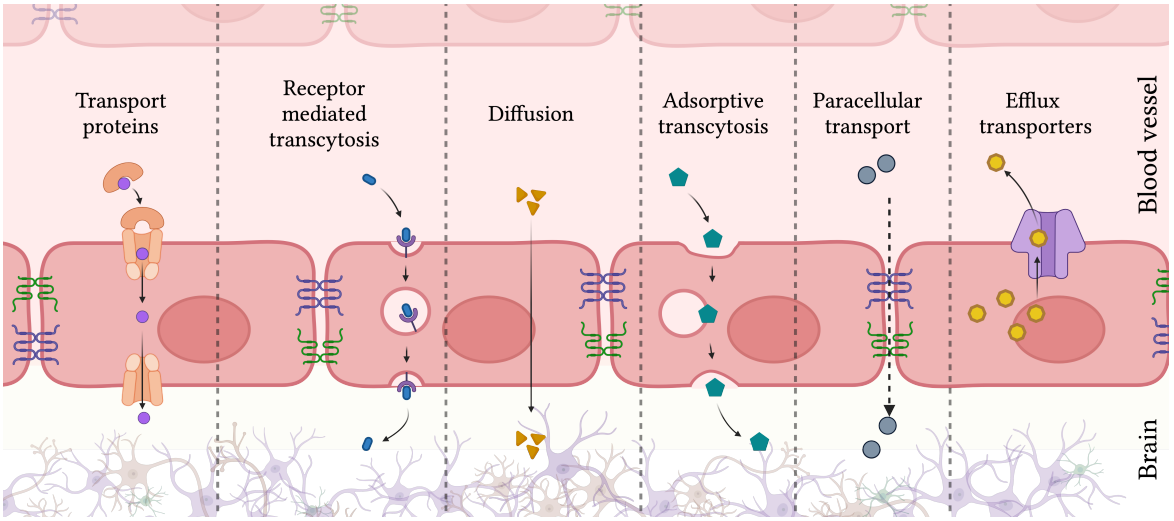

Figure 1.2: Transport pathways across the blood-brain barrier: Different transport mechanisms across the BBB. This figure was inspired by (Wu et al., 2023) and made in BioRender.com.

1.6 Magnetic nanoparticles

Magnetic nanoparticles (MNPs) are nanomaterials that consist of magnetic elements, such as iron, nickel or cobalt. They can vary in size from 1-100nm and they are characterised by their magnetic properties. (Flores-Rojas et al., 2022) Generally, MNPs sized <100nm pose superparamagnetic abilities making them highly magnetizable under a strong external magnetic field which disappears in the absence of this magnetic field. (Flores-Rojas et al., 2022) Their magnetic properties allow them to function as ferrofluids, and they have low toxicity due to their iron oxide core which degrades in the body to Fe^{2+} and Fe^{3+} (Boyer et al., 2010; Skotland et al., 2010). This makes them an excellent candidate for clinical application. Targeting MNPs to a certain organ or tumour provides a much clearer contrast agent magnetic resonance imaging (MRI) application (Billotey et al., 2003), as well as a great candidate for cell marking (Högemann et al., 2002). The magnetic properties

of the MNPs also allow for hyperthermia treatment by exposure to an external magnetic field the MNPs will heat up and kill the surrounding cells (Moroz et al., 2002). MNPs are also highly modifiable which qualifies them for drug delivery of both therapeutics and genes (Fortin et al., 2008; Stueber et al., 2021). Furthermore, MNPs constitutes some surface charge (measured in mV) that defines the electrokinetic potential of the particle, also known as the zeta potential. A measurement of the zeta potential is often used to determine the stability of a suspension of particles (Kędzierska et al., 2021). Zeta potential values higher than +30mV and lower than -30mV shows good stability of the suspension. Contrary, there is a tendency towards agglomeration as the zeta potential equals 0mV (Raval et al., 2019).

1.6.1 Coating of the MNPs

The magnetic core of the MNPs can be coated with different biomaterials to enhance both visual detection and bioavailability in the body (Flores-Rojas et al., 2022) (see fig 1.3). The coating is responsible for stabilising and protecting the core from the effects of the medium or biological material it contacts. (Flores-Rojas et al., 2022) Coating of the magnetic core can be done with several different biomaterials, such as phospholipids, polythene glycol (PEG), starch, polysorbate, dextran or glucuronic acid (Denizot et al., 1999; Kumar et al., 2010; Yallapu et al., 2010). Coatings first of all provide a protective barrier around the MNPs that prevents aggregation, and a shielding effect from the surrounding environment (Selim et al., 2024). This protection ensures the integrity and proper function of the particle to ensure their desired properties for drug delivery. Secondly certain coatings like PEG help by reducing recognition and clearance by the immune system (Suk et al., 2016). Coatings can also help to mitigate adverse immune responses and cytotoxic effects making them safer for clinical application. Additional coatings with antibodies or peptides allow for targeted delivery to desired areas of the body (Cheng et al., 2023; Selim et al., 2024).

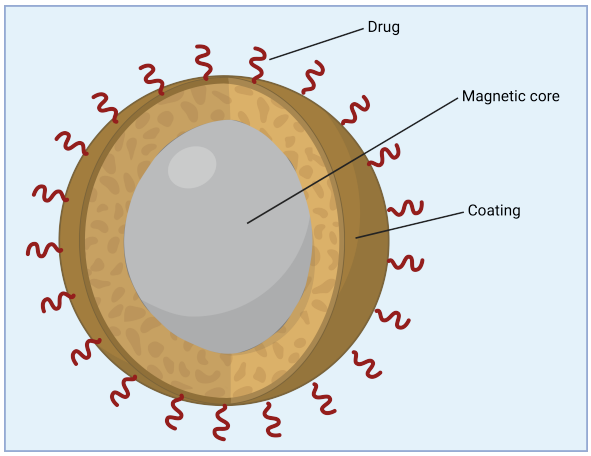

Figure 1.3: A simple illustration of the components of a magnetic nanoparticle: MNPs used for drug delivery are typically made up of a magnetic core, such as iron oxide, coated with a biocompatible polymer and finally conjugated with a drug of choice. This figure was made in BioRender.com.

1.6.2 Magnetic drug delivery systems

The pioneering idea posed by Freeman et al. (Freeman et al., 1960) that fine iron particles could be administered through the vascular system to a desired location in the body by the force of an external magnetic field , has since spread to much of the current research especially regarding cancer research and drug delivery (Goodwin et al., 1999). The use of magnetically guided nanoparticles has been studied in several different pathological conditions like tumours, inflammation and infection sites (Allafchian & Hosseini, 2019; Farzin et al., 2020). Commonly for these pathology's is a more permeable vasculature in these areas allowing for easier access in for macromolecules and nannoparticles due to the abnormalities of the vasculature (Maeda et al., 2000).

Over the past two decades, more attention has focused on nanoparticles for drug delivery (Yusuf et al., 2023). The small size coupled with a naturally low toxicity make MNPs a great candidate for a drug delivery system. They are easily modifiable for specific targeting making drug delivery more efficient (Fortin et al., 2008). The coating of the particles and the ability to conjugate therapeutics help make a more targeted approach (Hosu et al., 2019). Targeted drug delivery is highly efficient and has far fewer side effects than some conventional treatments. (Flores-Rojas et al., 2022; Hosu et al., 2019) Drug delivery using superparamagnetic MNPs holds a major advantage due to the ability to direct the MNPs to the desired site of treatment using a magnet. Once the magnetic field is removed, when the external magnetic field is removed, the MNPs do not retain their magnetisation, helping to prevent the formation of aggregations (Flores-Rojas et al., 2022). MNPs can be administered intravenously, due to their small size, and thereby be distributed throughout the body and to the target(Flores-Rojas et al., 2022; Kong et al., 2012; Lim et al., 2013) (see figure 1.4. Drug delivery using MNPs is very beneficial in cancer treatment. Traditional chemotherapy drugs are designed to act on cancer cells, but due to their toxicity, they will also harm healthy tissue. MNPs can localise the treatment and thereby reduce side effects (Flores-Rojas et al., 2022; Materón et al., 2021).

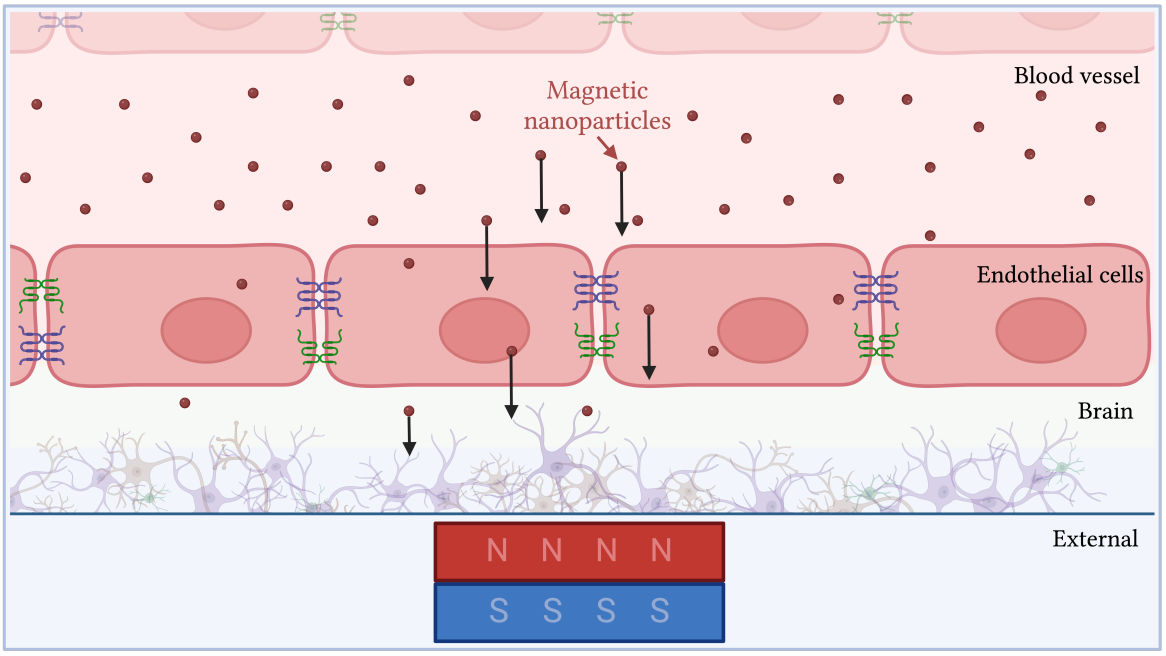

Figure 1.4: Magnetic field induced transport of MNPs over the blood-brain barrier. MNPs used for drug delivery are typically made up of a magnetic core, such as iron oxide, coated with a biocompatible polymer and finally conjugated with a drug of choice. This illustration visualise the idea of targeting MNPs to a specific tissue in the brain by using an external magnetic force. This figure was made in BioRender.com.

1.7 Aim

Based on the theories presented above, it is hypothesised that MNPs will pass the BBTB, influenced by GBM, to a greater extend that than a healthy BBB. MNPs are both in theory and practice good candidates for drug delivery to the brain. Multiple studies successfully have investigated the transport of MNPs across the BBB both *in vitro* and in vivo in healthy BBB models (Chen et al., 2022; Ding et al., 2014; L. B. Thomsen et al., 2013; X. Zhao et al., 2016). Additionally it is hypothesised that the influence of a magnetic field will facilitate a greater passage of MNPs.

Thus, this study aims to evaluate the passage of MNPs through an *in vitro* BBTB model with GBM. It is investigated weather there is a difference in the passage of MNPs over the BBTB both under the influence and absents of an external magnetic field of varying strengths. Additionally, it will be evaluated to what extend the MNPs are endocytosed by the endothelial cells. The passage of MNPs will be examined in a primary *in vitro* BBTB model using a co-culture of either porcine brain endothelial cells (PBECs) or human brain endothelial cells (HBMECs) and human GBM cells (T10) and a secondary control model using U87 cells. The passage of the MNPs will be evaluated by fluorescent microscopy as well as Perl's prussian blue analysis.

Methods

2.1 Project process

This section will be used to explain the intended plan for this project, providing the reader with an understanding of the decisions and changes made during this project.

The initial and overall purpose of this project was to provide research in targeted drug delivery for GBM. Firstly, the plan was to classify the GBM cell line T10, and try to find a good target for drug delivery (fig. 2.1.1). *In vitro* BBB and BBTB models were used to study the delivery of the targeted therapeutics to the GBM cells. At first, porcine brain endothelial cells (PBECs) were chosen due to their high integrity posing as a good comparative barrier for drug transport an in vivo barrier (fig. 2.1.2). Nano-screenMAG-D nanoparticles (red fluorescent MNPs) were used for this setup with the plan to quantify the MNPs crossing the barrier using fluorescent microscopy. However, these particles resulted in the destruction of the BBB and BBTB (fig. 2.1.3). Since, the nano-screenMAG-D nanoparticles were not in production anymore, the fluidMAG-ARA particles were purchased. These MNPs were non-fluorescent, but were conjugated with red fluorescent antibodies (fluidMAG-ARA+Ab). A cell viability assay was performed using the new MNPs. In the preparation for the next BBB/BBTB model, the isolation of PBECs failed multiple times. However, after much consideration, the project proceeded using HBMECs instead of PBECs. (fig. 2.1.4). The fluorescent microscopy analysis, following treatment of HBMEC BBB/BBTB models with fluidMAG-ARA+Ab nanoparticles, under the influence or absence of a magnetic field, did not indicate that any particles passed through the barrier. (fig. 2.1.5). Following this, fluidMAG-ARA particles without red fluorescent antibodies were tested and quantified by the perls prussian blue method. No particles seemed to cross the BBB/BBTB *in vitro* following the analysis of the medium from the bottom wells (fig. 2.1.6). Finally, the same setup as for the BBB/BBTB model with fludMAG-ARA was made, using an insert with no cells. This was to investigate whether it was the semipermeable membrane of the insert, or the endothelial cells preventing the particles from passing the barrier (fig. 2.1.7).

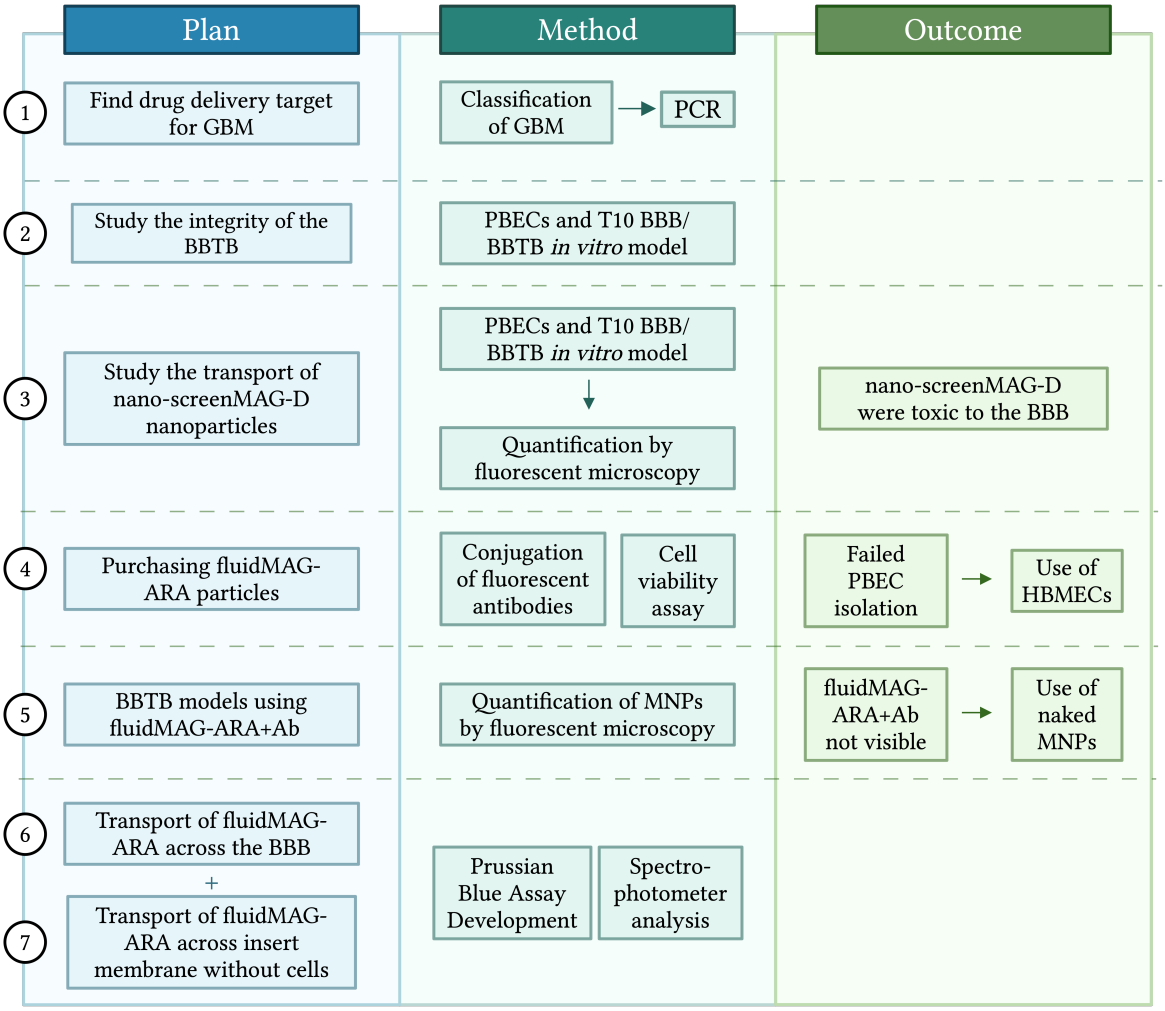

Figure 2.1: Schematic Overview of Project Process: The left column "*Plan*" illustrates the different plans and focus points considered during the project. The middle column "*Method*" illustrates the main methods and *in vitro* setups used. Finally the right column "*Outcome*" illustrates certain outcomes leading to a change of plan in the project. The numbers on the left illustrates the order of the events. *Glioblastoma Multiforme (GBM), Polymerase Chain Reaction (PCR), Blood-Brain Barrier (BBB), Blood-Brain-Tumour Barrier (BBTB), Porcine Brain Endothelial Cells (PBECs), Human Brain Microvascular Endothelial Cells (HBMECs) and Magnetic Nanoparticles (MNPs). FluidMAG-ARA+Ab refers to the particle conjugated with red fluorescent antibodies. FluidMAG-ARA reffers to "naked MNPs" without conjugated antibodies.* This illustration was made in BioRender.com.

2.2 Cell cultures

Porcine brain endothelial cells

Porcine Brain Endothelial Cells (PBECs) were isolated from the brains of six month old pigs kindly provided by Danish Crown, Herning. The brains were transported on ice to the laboratory at Aalborg Univeristy. The isolation protocol was followed as described by Thomsen et al. (L. B. Thomsen et al., 2015).

Human brain microvascular endothelial cells

Human brain microvascular endothelial cells (HBMECs) were gifted from Kwang Sik Kim and isolated from a brain biopsy of an adult female with epilepsy and immortalised as described in Greiffenberg et al. (Greiffenberg et al., 1998). HBMECs from passage 16 were thawed from storage in a cryotank at -160°C and cultured in endothelial cell medium consisting of Dulbecco's Modified Eagle Medium/Nutrient Mixture F-12 (DMEM)/F12 (glutamax) with 10% Plasma-derived bovine serum (First link ldt), 10% Insulin-Transferrin-Selenium (ITS) (ROCHE), gentamicin (Lonza) and 1ng/ml basic fibroblast growth factor (bFGF) (ROCHE) freshly added.

GBM cell lines

GBM cells T10 were derived from a patient at Rigshiapitalet, Copenhagen, and kindly donated from Kræftens Bekæmpelse. U87 cells established from the Uppsala University, Sweden in 1968 (Dolgin, 2016). Both T10 and U87 were cultured in medium consisting of Neurobasal™-A Medium (Gibco) with N2 supplement solution (x100) (Gibco) and B27- supplement without Vitamin A (50X) (Gibco), Glutamin- L 200 mM (Gibco), Penicillin/streptomycin solution (x100) (Gibco), bFGF at 25ng/ml and epidermal growth factor (EGF) (Sigma) at 25ng/ml (This medium will be referred to as GBM cell medium). The cells were thawed from storage in a cryotank at -160°C and cultured in T75 flasks with 15 ml medium per flask. These cells were thawed at the beginning of the experimental period and kept in culture during the entire period. Cell medium was changed once a week by pelleting the cells at 1200rpm for 5 minutes and resuspending them in fresh GBM cell medium.

2.3 *In vitro* transwell blood-brain barrier model

The *in vitro* BBB model setup consisted of a 12-well plate coupled with transwell hanging inserts with a pore size of 1µm and a surface area of 1,131 cm^2 (Corning, Thermo Fisher Scientific) (see figure 2.2). PBECs were seeded on transwell hanging inserts immediately following the isolation. HBMECs were thawed and cultured at least two weeks before use in a BBB setup. Both were seeded at a density of approximately 100,000 cells/cm^2 in both mono- and co-culture BBB setups. The insert membranes were coated with four parts sterilised water, one part fibronectin (SIGMA) and five parts collagen IV (SIGMA) at least one hour before seeding cell unto them. Endothelial cells were seeded onto coated inserts at day 0 and incubated overnight in a humidified incubator with 5% CO_2 at 37°C. Likewise were GBM cells cultured in 12-well plate at approximately 60.000 cells/cm^2 on day 0 and incubated overnight. To induce BBB characteristics endothelial cells (at day 1) in the transwell insert was washed twice with PBS followed by adding fresh endothelial cell medium including inducing factors of 17,5µM RO 20-1724 (RO), 250µM cyclic AMP (cAMP) (SIGMA) and 550nM hydrocortisone (HC) (SIGMA). The medium in the bottom chamber was also replaced with fresh medium containing 550nM HC. For the

mono-culture only endothelial cell medium was added. For the co-culture, a mix of endothelial and GBM cell medium was added (1:1). At this time the inserts containing endothelial cells were moved to the 12 well plates containing the GBM cells and incubated for approximately one week.

2.4 Transendothelial electrical resistance measurements

The barrier's integrity was evaluated by measuring and calculating the Transendothelial Electrical Resistance (TEER) value. TEER measurements were conducted with a Millicell ERS-2 apparatus (Millipore) and an STX-1 electrode (Millipore). All measurements were made in triplicates and the average value from each well was used for further calculations. TEER was calculated by subtracting resistance, measured in Ω, in the control well ($W_{control}$) from the sample well (W_{sample}) and multiplying by the surface area of the insert (1,131cm^2). The formula is as follows:

$$(W_{control} - W_{sample}) \cdot 1,131 cm^2 = TEER(\Omega cm^2)$$

TEER was measured daily, starting at day 0, during the setup and fresh medium was only added with the MNPs. The control insert used consisted of a coated transwell insert without any cell culture.

2.5 Covalent coupling of MNPs and fluorescent antibodies

The magnetic nanoparticles used in this project are commercially available fluidMAG-ARA from Chemicell. They consist of iron oxide with hydrodynamic diameters of 100nm. The particles are covered with a polymer matrix of glucuronic acid. The particles were coupled with Goat Anti-Rabbit IgG H&L (Texas Red ®) (Abcam) using the following procedure.

The desired amount of fluidMAG-ARA particles was added to an eppendorf tube placed on a magnetic rack to separate the particles from the solution. Firstly fluidMAG-ARA particles were washed twice in 0,1M 2-(N-Morpholino)ethanesulfonic acid (MES) buffer (pH 5.0). A freshly prepared 1-ethyl-3-(3-dimethylaminopropyl) carboodiimide (EDC) at a final concentration of 0.209M in MES bufferr was added to the fluidMAG-ARA particles and incubated for 20 minutes at 200rpm at room temperature using a mixing table. Following the incubation, the activated particles were once again washed twice in MES buffer and resuspended in MES buffer. The particles were now prepared for coupling with a fluorescent antibody, Goat Anti-Rabbit IgG H&L (Texas Red ®). Particles were mixed with 50µg of the antibody and incupated for 2 hours at room temperature on a mixing table at 150rpm. Finally the conjugated particles were washed thrice in PBS and stored in storage buffer consisting of 0.1% BSA in PBS.

2.6 Size and charge of the MNPs

The size and zeta-potential of fluidMAG-ARA with and without antibodies conjugates were measured by dynamic light scattering (DLS) using a Zetasizer Nano apparatus (Malvern Instruments; Malvern, UK) at Agro Food Park, Aarhus University, Denmark. To perform the measurements of size and zeta-potential the MNPs were loaded at 20µg/ml of distilled water to a glass cuvette and folded capillary zeta cell respectively. The hydrodynamic diameter of the MNPs was calculated by the Zetasizer Advance - ZS Xplorer software update v3.31. All measurements were made at room temperature in triplicates.

2.7 Cytotoxicity of fludMAG-ARA nanoparticles on HBMECs, T10 and U87 Cells

To examine the cytotoxic effect of the MNPs both the HBMECs, T10 and U87 cells a viability setup was made using different concentrations of MNPs. Cells were seeded in triplicates in a 48-well plate at approximately 100,000 cells/well one day before treatment. Cell viability was examined using trypan blue dye (Bio-Rad) and a hemocytometer. Five treatment groups were made: Dimethylsulfoxide (DMSO) (SIGMA), no treatment, and a final concentration of MNPs of 35, 70, and 140µg/mg respectively. The cells were incubated with or without MNPs in a humidified incubator with 5% CO_2 at 37°C for 24 hours. Following the incubation, cells were trypsinised and mixed with trypan blue. All live and dead cells were counted under a microscope.

2.8 Magnetic nanoparticles applied to BBB/BBTB model

A total of five experimental setups for MNP transport across the BBB were made. An overview of different setup constellations made in this study can be found in table 2.1, including cell type, magnet exposure time, magnetic field strength, MNP type and MNP concentration. In all setups, the MNPs were added approximately one week after endothelial cells in BBB/BBTB models were induced. This time allowed for barrier formation of the endothelial cells indicated by a plateau in TEER values. The MNPs were added in doses of either 35, 70, or 140 µg/ml. The MNPs were added in triplicates to the transwell inserts and incubated for 24 hours. In setup 1-3 the magnet-exposed plates were placed on the given magnet immediately following the addition of the MNPs. The magnet-exposed plates in setup 4 and 5 were left for 2 hours, following the MNP treatment, before being placed on the magnet for 20 minutes. This was done to ensure sedimentation of the particles before exposure to the magnetic field. A general overview of the process of adding MNPs to the BBB/BBTB model and exposure to a magnetic field is illustrated in figure 2.2.

Table 2.1: Overview of the different BBB models made in this study including magnet size measured in tesla (T), Magnet time on the BBB model, type of magnetic nanoparticle and concentration of the given nanoparticle.

Setup	BBB model	Magnetic field	Magnet time	MNP type	MNP concentration
1	PBECs	0.39T	30 min	Nano-screenMAG-D	70µg/ml
2	HBMECs	0.39T	30 min	fluidMAG-ARA+Ab	35, 70, 140 µg/ml
3	HBMECs	0.39T	5 h	fluidMAG-ARA+Ab	70µg/ml
4	HBMECs	1T	20 min	fluidMAG-ARA	140µg/ml
5	No cells	1T	20 min	fluidMAG-ARA	140µg/ml

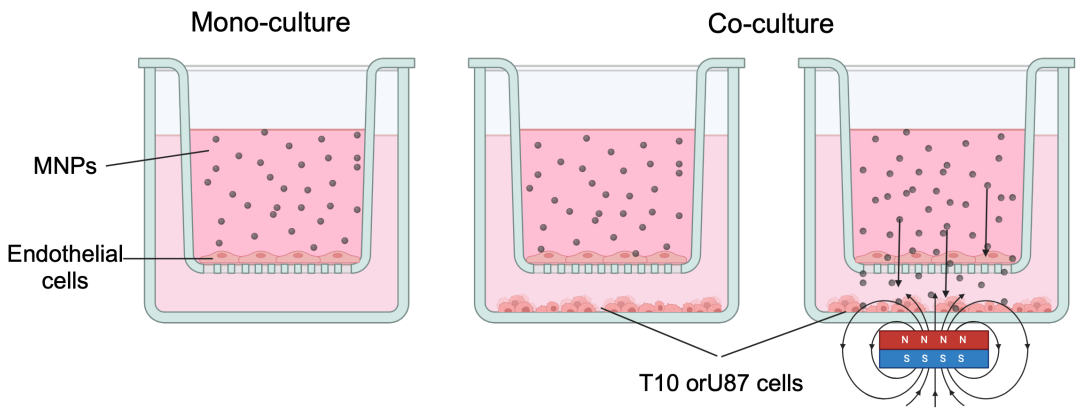

Figure 2.2: Blood-Brain Barrier Model: Illustration of BBB setup treated with MNPs. Mono-culture only has endothelial cells in the insert. Co-cultures have both endothelial cells and T10 or U87 cells seeded in the bottom well. One co-culture model is treated with a magnet. This figure was made in BioRender.com.

2.9 Perl's prussian blue stain

Following the BBB experiment, the concentration of the MNPs was measured based on their iron content. This measurement is based on the Perl's Prussian Blue reaction which allows for blue staining of an iron-containing solution when digested by hydrochloric acid (HCL) and potassium ferrocyanide (Boutry et al., 2009). This principle is based on the fact that potassium ferrocyanide reacts with the ferric chloride in the solution to form ferric ferrocyanide, also known as Prussian blue. This complex is characterised by a strong absorbance around 650nm. The absorbance of the samples was measured using the Multiscan SkyHigh (Thermo Fisher Scientific). The protocol for this method was inspired by Thomsen et al. (L. B. Thomsen et al., 2019). All medium samples, from inserts and bottom wells, were centrifuged for 5 minutes at 20,000xg followed by carefully removing the supernatant using a pipette leaving no more than 100µl in the eppendorf tube. Hereafter, 200µl 5N HCL was added to each sample and incubated at 80°C for 4h at 450rpm using a thermomixer (Eppendorf). Finally, 200µl of 5% potassium ferrocyanide was added to each sample and incubated for 15 min. at room temperature. The absorption for each sample was measured at 650nm. All samples were measured in triplicates.

To determine the iron concentration of each sample, a standard curve was made. Concentrations were made by adding 80µg MNPs in 400µl HCL and diluting it using dilution factor 1:2 six times. A standard curve was made and used to calculate the concentrations of the MNPs in the experimental samples.

2.10 Immunocytochemistry

After finalising a BBB setup, endothelial cells in the hanging transwell inserts were fixated using 4% paraformaldehyde for 5 minutes followed by two washes in PBS. Before antibody treatment, all samples were blocked using a blocking buffer of 3% BSA + 0.3% Triton X-100 in PBS for 1h at room temperature. HBMECs were incubated overnight at 4°C with rabbit anti-ZO-1 (Thermo Fisher, USA) and T10 and U87 cells with mouse anti-vimentin (DAKO). Following the incubation all samples were washed thrice in washing buffer made from 2% blocking buffer in PBS. To visualise the primary antibodies HBMEC were incubated with Alexa flour 568 goat anti-rabbit (Invitrogen) and Alexa flour 488 donkey anti-mouse antibody (Invitrogen) respectively. Finally, all samples were stained using 4',6-diamidino-2-phenylindole (DAPI) solution diluted 1:500 in PBS. Primary and secondary antibodies were diluted 1:500 in the blocking buffer. Following the DAPI staining all membranes were carefully cut out from the hanging inserts using a scalpel, and mounted on object slides using DAKO fluorescent mounting medium.

2.11 Fluorescent microscopy

Mounted cells were examined using Zeiss Observer.Z1 inverted fluorescence microscope (Zeiss). All images were taken using the Zeiss Zen Pro 3.1 software and all image processing and editing were done in Fiji imageJ (Schindelin et al., 2012).

2.12 Primer design

Primers were designed using the Primer BLAST tool (Ye et al., 2012).

Table 2.2: Sequences of primers used in this study. *Hypoxanthine Phosphoribosyltransferase 1 (HPRT1), Low-Density Lipoprotein Receptor-Related Protein 1 (LRP1), Transferrin Receptor (TfR), Epidermal Growth Factor Receptor (EGFR), Platelet-Derived Growth Factor Receptor (PDGFR), and Tumor Protein P53 (TP53)*

Gene	Sequence 5′ → 3′	Amplicon Size (pb)
HPRT1	Fw: 5′-GCCCTGGCGTCGTGATTAGT-3′ Rv: 5′-TGGCCTCCCATCTCCTTCATCA-3′	-
β-actin	Fw: 5′-CCGCCGCCAGCTCACCAT-3′ Rv: 5′-GCCCCACGATGGAGGGAAAG-3′	-
LRP1	Fw: 5′-CACACGCCAACTGCACCAAC-3′ Rv: 5′-ACGTGGGTCACTCCCTCACA-3′	169
TfR	Fw: 5′-GAGGACGCGCTAGTGTTCTTCT-3′ Rv: 5′-GCCAGGCTGAACCGGGTAT-3′	114
EGFR	Fw: 5′-CTGGGGTGCAGGAGAGGAGA-3′ Rv: 5′-TCGGAATTTGCGGCAGACCA-3′	169
PDGFR	Fw: 5′-GTGGTGAGCACACTGCGTCT-3′ Rv: 5′-AGGGCCAGGATGGCTGAGAT-3′	152
TP53	Fw: 5′-TGCTTTCCACGACGGTGACA-3′ Rv: 5′-GGATCTGACTGCGGCTCCTC -3	87

2.13 RNA isolation, cDNA synthesis and real-time qPCR analysis

Before the RNA purification T10 and U87 cells were seeded in triplicates in T25 flasks at approximately 1.4 x 10^6 cells. RNA was extracted from both cell lines using the Thermo Scientific GeneJET RNA Purification Kit (#K0732). Following this, genomic DNA was removed from RNA purifications using DNase I, RNase-free Pub. No. MAN0012000 (Thermo Fisher). All purified RNA was stored at -20°C until cDNA synthesis. Single-stranded cDNA was synthesised using Thermo Scientific Maxima H Minus First Strand cDNA Synthesis Kit (#K1651) in a 20µl reaction as advised by the manufacturer's instructions and stored at -20°C until use.

Standard curves were made for the following genes: LRP1, TfR, EGFR, PDGFR and TP53. Each standard curve was prepared from a 10-fold dilution series with a pool of cDNA from all samples at a concentration of 2ng/µl. The samples were diluted five times. RT-qPCR was performed using 5µl of prepared cDNA (0.4ng/µl), 5µl SYBERgreen and 0,03µl of fw and rv primer respectively.

cDNA samples were added at a concentration of (0.4ng/µl) mixed with 5µl SYBERgreen and 0.03µl of fw and rv primer respectively and analysed using the QuantStudio 6 Flex (Thermo Fisher) and the QuantStudio 3/5 Real-Time PCR Software (Thermo Fisher). Calculations of the relative gene expression were done using the Pfaffel method (Pfaffl, 2001) using β-actin and HPRT1 as housekeeping genes.

2.14 Statistical analysis

All data from all experiments are presented as the mean ± standard deviation (SD). A parried or unpaired students t test was used to compare means of TEER values before and after treatment, and for the relative gene expression of T10 cells. Significant difference for the cell viability test was analysed using a one-way ANOVA with Tukey's multiple comparison post hoch test for the U87 cells. Data from T10 and HBMEC was not normally distributed and therefore analysed using Kruskal-Wallis test with Dunn's multiple comparison post hoc test. All data analysis including graphs, means, SD, and p values were calculated with the Graphpad Prism 7 software. Statistical significant differences are indicated as *P<0.05, **P<0.01, ***P<0.001 and ****P<0.0001.

Results

3.1 Classification of the T10 cell lines

The genes chosen for RT-qPCR reflect some of the important cellular processes that can take place in GBM tumours. Since the U87 cell line is a commonly used cell line for GBM studies, this cell line was used as a control for measuring the relative gene expression of T10 cells. Following RNA isolation, cDNA synthesis and RT-qPCR analysis the relative gene expression was calculated based on the CT values using the Pfaffel method. Comparing the means, using an unpaired t-test, resulted in a significant difference between all genes expressed in T10 cells in relation to U87 cells. LRP1 (P=0.0021), TfR (P=0.032), PDGFR (P<0.0001) TP53 (P<0.0001), and EGFR (P=0.0004) (see figure 3.1).

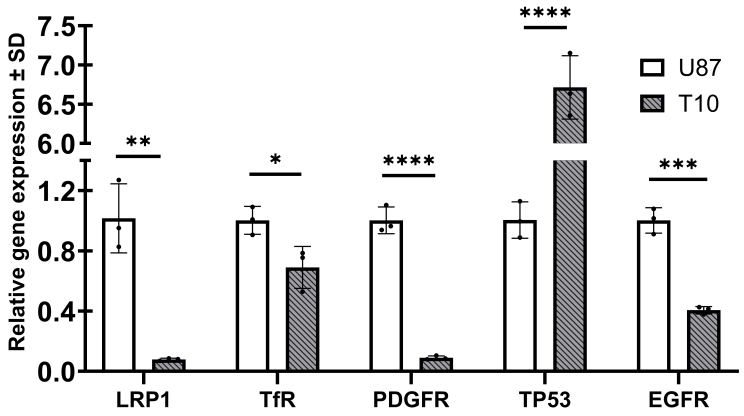

Figure 3.1: Relative gene expression of GBM cell markers in T10 cells. RT-qPCR analysis of relative gene expression comparing T10 cells to U87 cells. Prior to RNA purification, T10 and U87 cells were cultured respectively in 3 different cultures in GBM cell medium for a week. Data is expressed as the mean ± Standard deviation (SD). An unpaired t-test was used to compare means of each gene expression compared to the control. N=3 for all samples. *Low-Density Lipoprotein Receptor-Related Protein 1 (LRP1), Transferrin Receptor (TfR), Epidermal Growth Factor Receptor (EGFR), Platelet-Derived Growth Factor Receptor (PDGFR), and Tumour Protein P53 (TP53).*

3.2 Determining the length of the integrity for blood-brain and blood-brain-tumour barrier model

The BBB and BBTB *in vitro* model using PBECs for the mono-culture BBB and PBECs and T10 for the co-culture BBTB was a pilot study, made to determine the integrity of the BBTB over time compared to the BBB. Results helped to be able to determine the optimal time for treatment with MNPs, being when the barrier was at a high and stable TEER integrity. In fig 3.2 a. a mean of TEER measurements for both the mono- and co-culture with T10 are presented. Following the induction of both barriers the TEER values rose from 57.1 Ω

x cm^2 ±19.3 and 55.4 Ω x cm^2 ± 18.6 to 254.0 Ω x cm^2±54.1 and 449.5 Ω x cm^2 ± 125.4 for the mono- and co-culture respectively. Peak TEER values were seen 5 days after induction for the mono-culture and 4 days after for the co-culture at 472 Ω x cm^2 ± 65.6 and 848.6 Ω x cm^2 ± 90.0. Both BBB models seemed to plateau for about three days around their max TEER value. At day 9 fresh media was added to both the inserts, and the bottom wells, which for the co-culture resulted in a spike in TEER from 637 Ω x cm^2 ± 66.3 to 785.0 Ω x cm^2 ± 74.4. No increase in TEER was observed for the mono-culture as a result of adding fresh media. At about two weeks after induction of the barrier the integrity of the mono-culture was about the level that it was at the start of the experiment. This BBB setup was ended after three weeks where the co-culture presented with TEER values similar to the one at day 2.

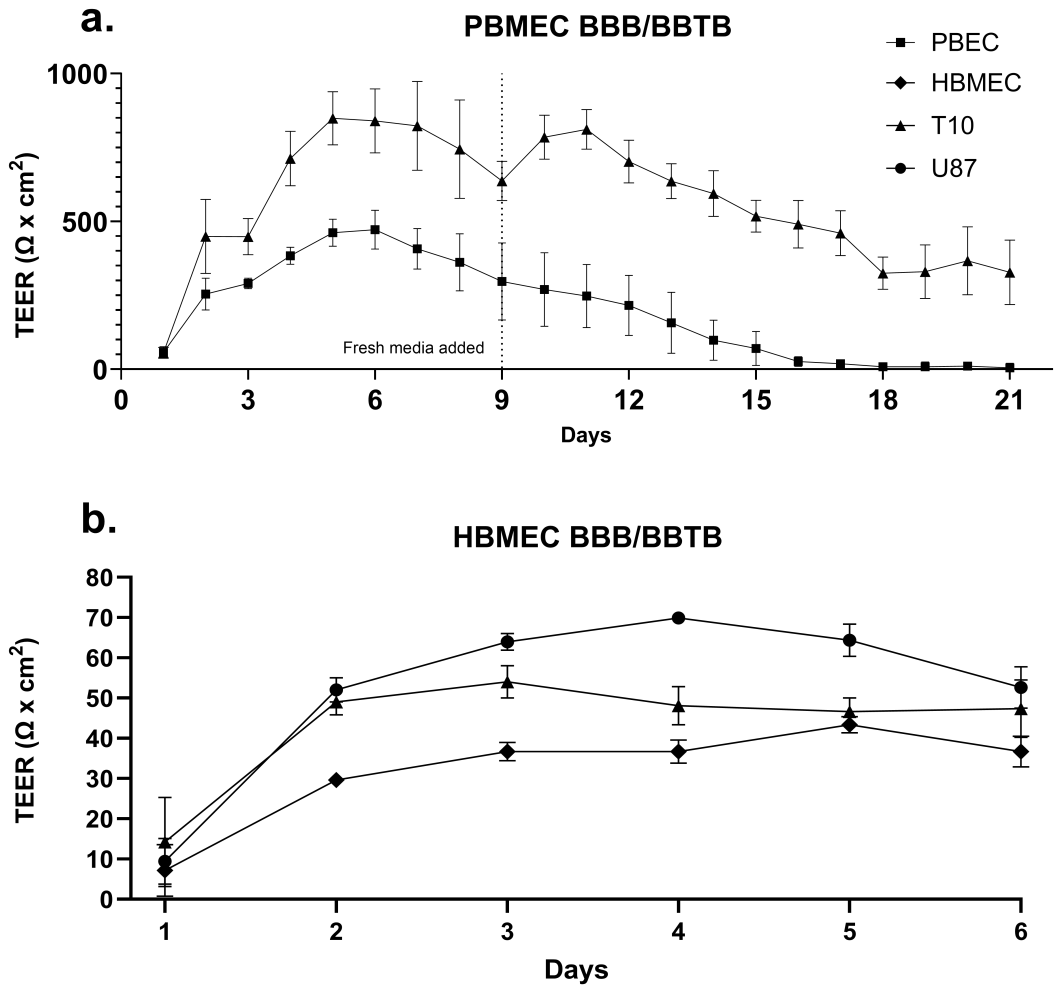

Figure 3.2: TEER Measurements for Mono- and Co-culture BBB and BBTB a. Measured TEER value (Ω x cm^2) means ±SD for BBB mono-culture with PBECs (squares) and BBTB co-culture with PBECs and T10 cells (triangles). At day 9 fresh medium was added as represented by the dotted line. **b.** TEER values ±SD for BBB mono-culture with HBMECs (dimond) and BBTB co-culture with HBMECs and T10 or U87 (circle) cells.

In fig 3.2 b. TEER measurements are visualised from a similar BBB/BBTB model using HBMECs instead of PBECs. This setup included co-cultures with either T10 or U87 cells. Following the induction of both barriers the TEER values rose from 7.2 ±6.4Ω x cm^2 to 29.7 ±1.4Ω x cm^2 for HBMECs, 14.2 ± 11.1Ω x cm^2 to 14.2 ±11.1Ω x cm^2 for BBTB with T10 cells and 9.4 ±5.7Ω x cm^2 to 52.0 ±3.0Ω x cm^2 for BBTB with U87 cells. Peak TEER values at 43.4 ±2.0Ω x cm^2, 54.0 ±4.0Ω x cm^2 and 70.0 ±1.0Ω x cm^2 respectively.

Figure 3.3 illustrates immunocytochemical staining of PBECs compared to HBMECs. PBECs are stained for Claudin-5 and HBMECs for Z0-1. Although these are not thee same tight juntion proteins, the do provide an accurate outline of thee cells. It is clear to see the size difference between the two cells. PBECs are larger and create a uniform monolayer of cells. Whereas, HBMECs are much smaller and more confluent creating a polylayer in the insert membrane with some areas less dense than others, as seen with white arrows in figure 3.3 B3.

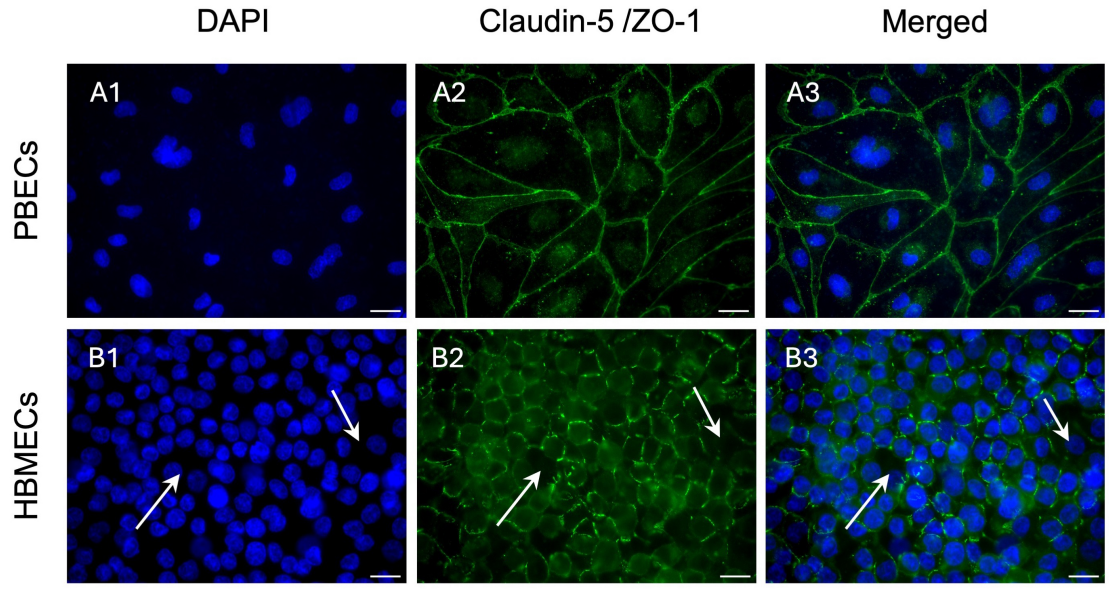

Figure 3.3: Fluorescence Images of PBECs and HBMECs Seeded on Transwell Inserts Represents images from mono-culture BBB model with either PBECs or HBMECs. PBECs are labeled with claudin-5 (alexa 488) (green) and HBMECs labelled with zonula occludens-1 (ZO-1) (Alexa 488) (green). The nuclei are stained with 4',6-diamidino-2-phenylindole (DAPI) (blue). White arrows point to areas where the cell layer is less dense. Scale bar = 50nm

3.3 Nano-screenMAG-D were toxic to *in vitro* BBB model

BBB and BBTB models treated with 70µg/ml nano-screenMAG-D with or without a magnet (30 minutes), had a significant decrease in TEER ($P<0.0001$; n=3) (see figure 3.4). Graphs visualising the full TEER measurements are shown in Appendix A figure A.1. Only the control, showed in figure 3.4 a., showed no significant difference in TEER values before and after treatment ($P>0.05$). Based on these results the use of nano-screenMAG-D

nanoparticles was discontinued.

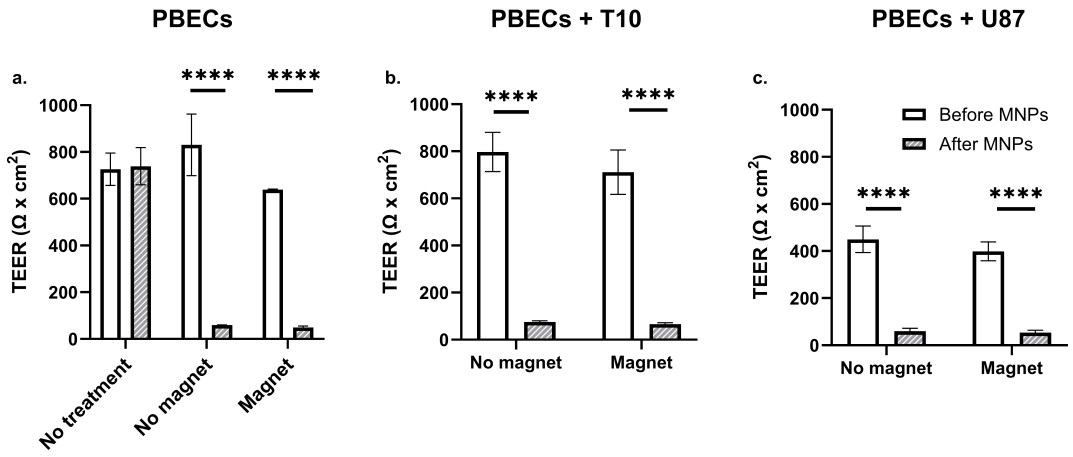

Figure 3.4: Transendothelial Electrical Resistance (TEER) measurements before and after treatment of BBB and BBTB using nano-screenMAG-D. Measured TEER value (Ω x cm^2) means ± SD for BBB mono-culture with PBECs (a.) and BBTB co-culture with PBECs and T10 cells (b.) or U87 cells (c.). All models were treated with 70µg/ml nano-screenMAG-D particles immediately after the TEER measurement before treatment (white bars). Plates not exposed to a magnet were incubated for 24 hours with the MNPs. Magnet plates were incubated for 30 minutes on a 0.39T magnet and off the magnet for the remainder of the 24 hours. TEER was measured again following the incubation (gray bars). N=3 for all groups.

3.4 Coupling of antibodies to fluidMAG-ARA nanoparticles

To visualise the successfully conjugation of the red fluorescent antibodies to the fluidMAG-ARA nanoparticles, 200µg of them, diluted in PBS, were placed with or without antibodies in a 48 well plate for fluorescent microscopy analysis (figure 3.5). Images were taken at the same intensity for each channel for both types of particles. Images show multiple speckles in the red channel for particles with antibodies compared to those without.

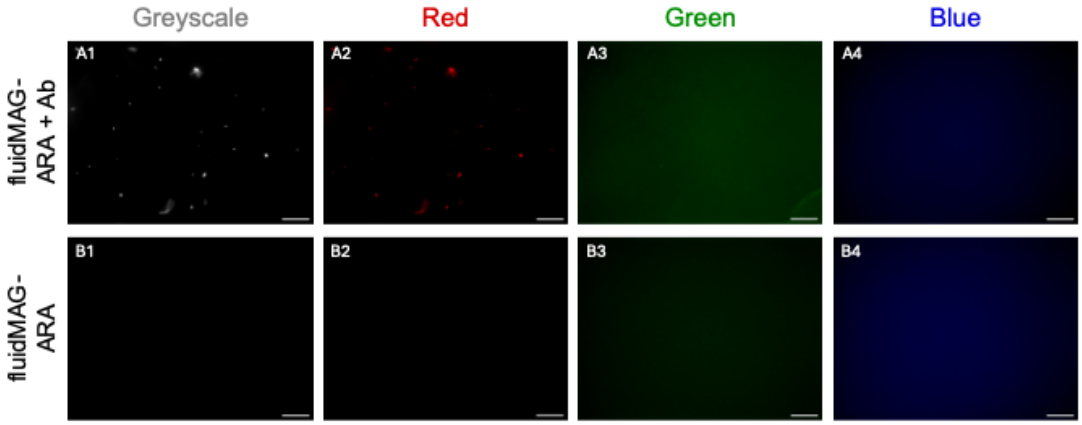

Figure 3.5: Fluorescence images of fluidMAG-ARA with and without antibodies Represents images from a 48-well plate with 200µg in PBS fluidMAG-ARA nanoparticels with and without conjugated fluorescent antibody. **A1-A4** FluidMAG-ARA with fluorescent antibody. **B1-B4** FluidMAG-ARA without fluorescent antibody. Column 1 is a grayscale of the red channel used for better visualisation of the MNPs. Column 2, 3 and 4 are the red, green and blue channel respectively. Scale bar = 50µm.

3.5 Size and charge of the fluidMAG-ARA nanoparticles

The hydrodynamic diameter was measured by Zetasizer measurement in triplicates with 10 measurements for each sample to a mean of 105.4±2.427nm fluidMAG-ARA and 263.5±23.97nm for fluidMAG-ARA+Ab. The zeta potential of both particles were measured to -35.35±1.845mV and -22.26±1.043mV (see table 3.1 and figure 3.6). The antibodies made the particles have a slightly more positive surface charge.

Table 3.1: Hydrodynamic size and zeta potential ±SD.

	Hydrodynamic size (nm)	**Polydispersity index (PDI)**	**Zeta-potential (mV)**
fluidMAG-ARA	105.4 ± 2.427	0.243 ± 0.0207	-35.35 ± 1.845
fluidMAG-ARA+Ab	263.5 ± 23.97	0.611 ± 0.0294	-22.26 ± 1.043

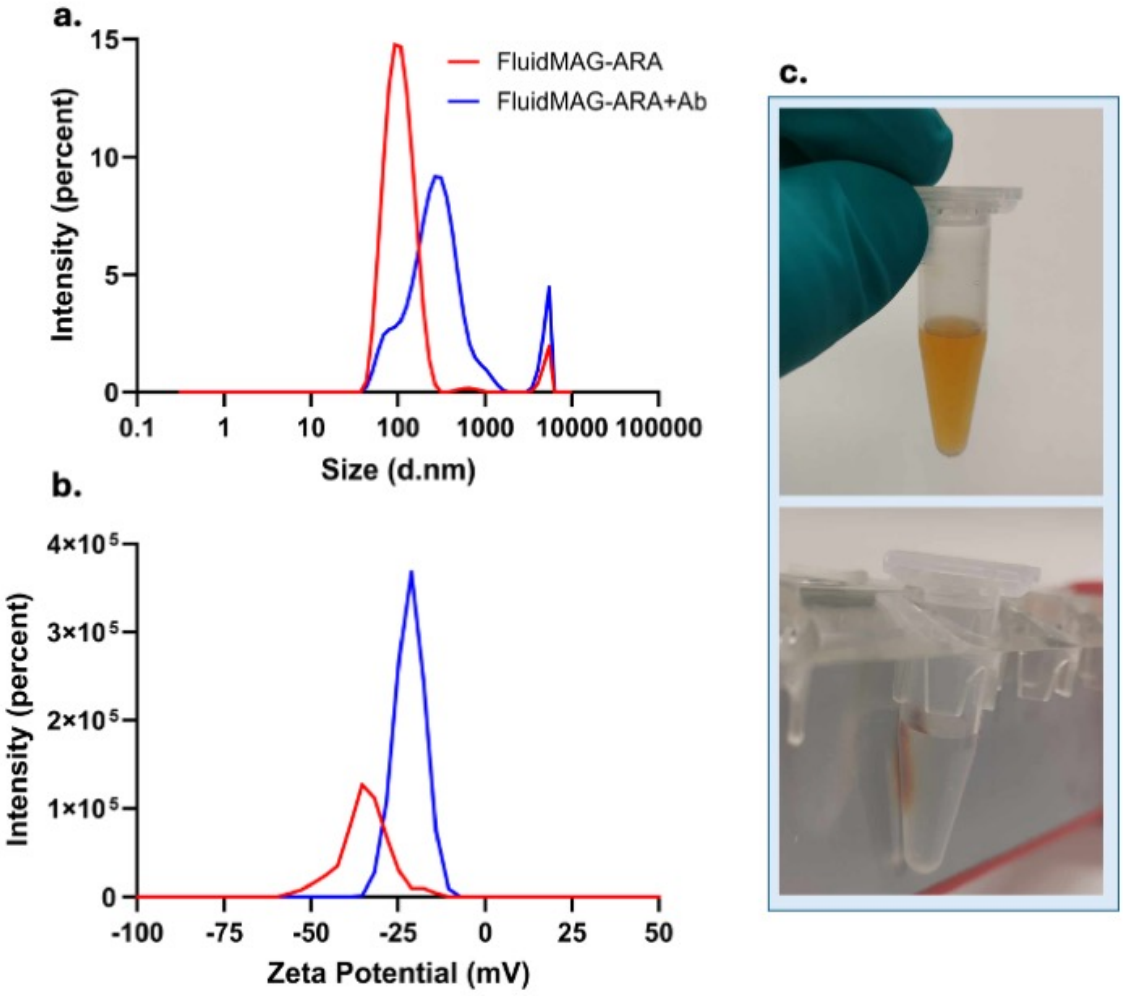

Figure 3.6: Hydrodynamic diameter and zeta potential for fluidMAG-ARA and fluidMAG-ARA+Ab (a.) The size of the particles are plotted on a log10 x-axis displaying the hydrodynamic size in nm. **(b.)** Zeta potential is displayed in mV with the intensity of particles in percent on the y-axis.**c.** Images of fluidMAG-ARA nanoparticles to illustrate their magnetic properties when influenced by an external magnetic field.

3.6 FluidMAG-ARA were not toxic to HBMECs, T10 or U87

Cell viability is estimated from a live/dead stain cell count 24 hours after given treatment and presented as the mean percentage of cell viability for HBMECs, T10 and U87 ± SD. HBMECs percentage viability remained unchanged by the particles (ranging from 99.4% ± 0.82 - 99.6% ± 0.8) with no surviving cells treated with DMSO (0%). Both U87 and T10 cells seemed to vary in general cell viability. Due to the cells formation in spheres and a characteristic necrotic cores, it was expected to observe more dead cells in the GBM cell lines compared to the HBMECs. U87 cell showed a significant difference between the "no treatment" group and the "treatment" group with 70 and 140µg/ml (P=0.0043, P=0.038) as well as between the cells treated with 35µg/ml to the groups with 70 and 140µg/ml (P=0.0006, P=0.007). No significance is seen between the treatment groups for T10 or HBMECs independently.

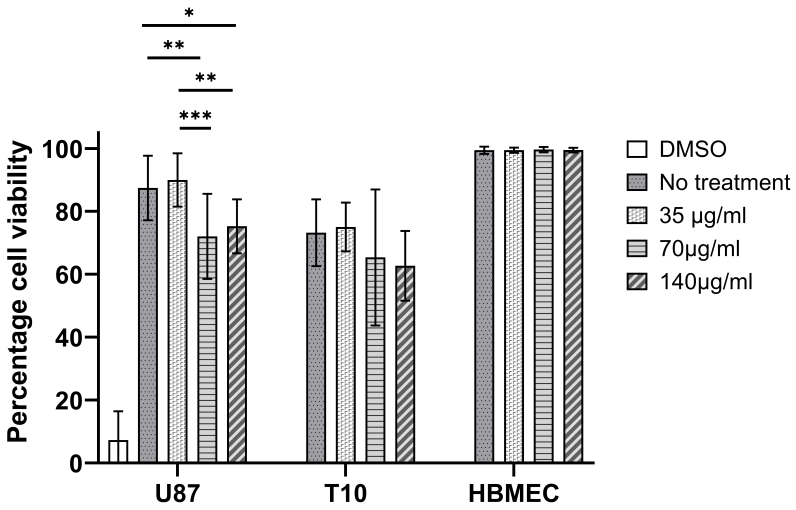

Figure 3.7: Cell viability assay with fluidMAG-ARA: Cell viability is illustrated for HBMECs, T10 and U87 cells shown in mean percentage cell viability ±SD. All cells were seeded and cultured three days before treatment. Each cell type received one of five treatments; DMSO (Control treatment), no MNPs, 35µg/ml, 70µg/ml and 140µg/ml, and they were incubated for 24 hours at 37°C. Following the incubation time all cells were counted using a hemocytometer. Data for U87 was normaly distributed and analysed using a one-way ANOVA with Tukey's multiple comparison post hoch test. Data from T10 and HBMEC was not normally distributed and theerefore analysed using Kruskal-Wallis test with Dunn's multiple comparison post hoc test. There was a significant difference between DMSO treatment and all other treatments for all the cell types (P<0.0001). N=3 for all samples

3.7 Different concentrations of fluidMAG-ARA+AB transported across the HBMEC BBB/BBTB

FluidMAG-ARA+AB was administered the HBMEC BBB model at different concentrations (35, 70 and 140µg/ml) to investigate the optimal concentration for future treatment. The TEER graphs for the full experiment can be found in appendix A figure A.1. Firstly the integrity of the barrier was not altered by any concentration of MNPs. Neither did the

presence of a magnetic field affect the integrity of the barrier before and after treatment as seen in figure 3.8. It is evident the TEER values increased following the treatment with MNPs for most treatment concentrations.

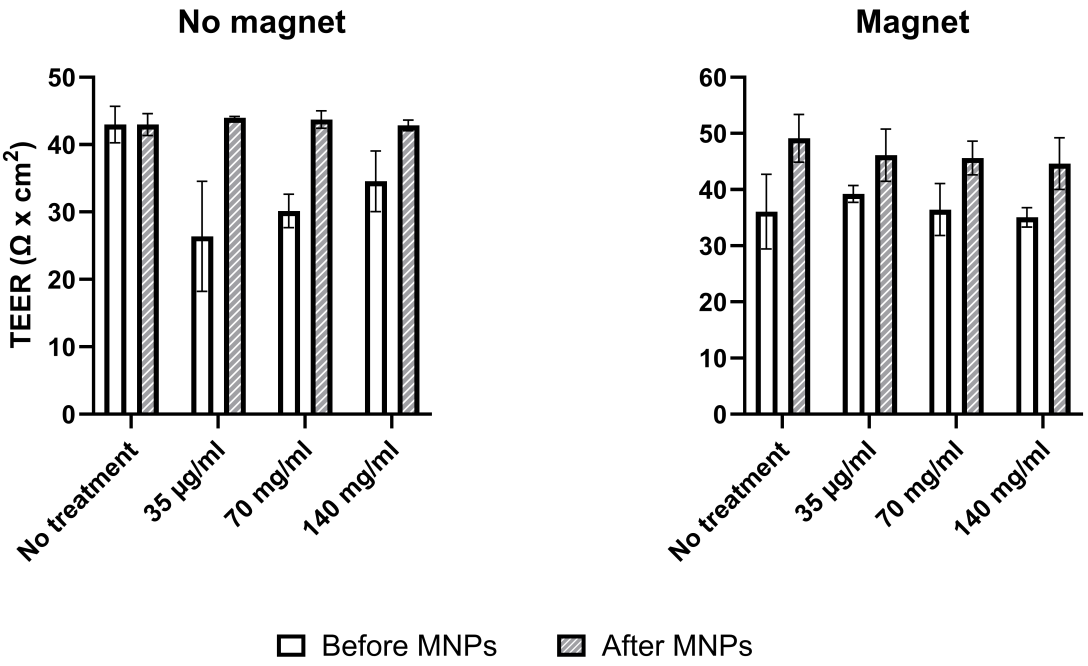

Figure 3.8: TEER measurements before and after administration of fluidMAG-ARA at different concentrations. Measurements of TEER values before and after treatment using different concentrations of fluidMAG-ARA particles (0, 35, 70 and 140 µg/ml). The BBB model is setup as a mono-culture of HBMECs incubated for 24 hours after treatment with MNPs. One was incubated without a magnet (a.) and the other plate was incubated 30 minutes on a magnet followed by 24 hours without (b.). TEER values (Ω cm^2) is visualised ad means ±SD(n=3).

Investigation of whether the MNPs crossed the barrier or not was done by fluorescent microscopy. The purpose of this was to quantify by counting the MNPs in the visual field of the microscope. As evident from figure 3.9, the MNPs were only visible in the medium extracted from the hanging inserts.

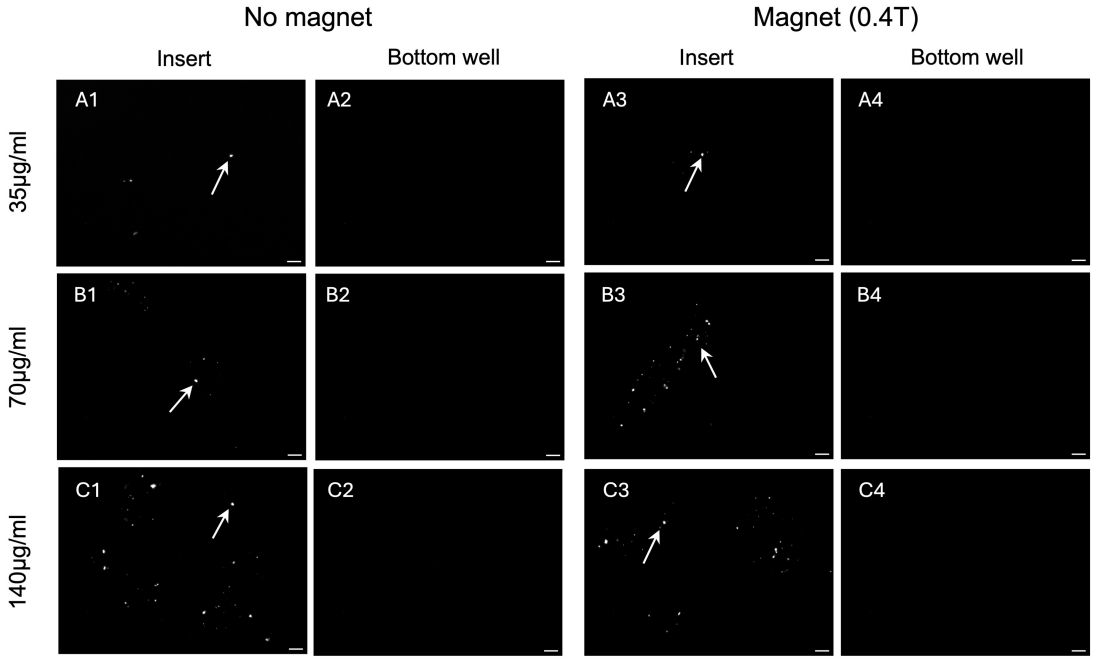

Figure 3.9: Grayscale fluorescence images of fluidMAG-ARA+Ab in Inserts and Bottom Wells. Fluorescence images of fluidMAG-ARA+Ab at different concentrations (35, 70 and 140µg/ml) in the medium of inserts or bottom wells with or without magnetic influence. All medium samples are from mono-culture HBMEC BBB models. Images are all presented in grayscale to better visualise the particles. White arrows point to the particles on the image. Scale bar = 50nm

3.8 Integrity of the BBB/BBTB was not altered by fluidMAG-ARA+Ab nanoparticles

For the third setup 70µg/ml fluidMAG-ARA+Ab were used with the magnet treated samples placed on the magnet for 5 hours. Figure 3.11 (a.-c.) present mean TEER values Ω cm^2 ±SD before and after treatment with MNPs. Both the BBB HBMEC mono-culture and BBTB co-culture with HBMECs and T10 or U87 showed no significant disruption in the integrity of the barrier caused by the treatment ($P>0.05$). Quantification using fluorescent microscopy resulted in no visual MNPs in the medium from the bottom wells, only from the inserts, similar to the results shown in figure 3.9. Further fluorescent analysis of the HBMECs were made to investigate to what degree the cells internalised the fluidMAG-ARA+Ab nanoparticles (see figure 3.10). The immunocytochemical images look similar for the three groups showing no signal from the fluidMAG-ARA+Ab nanoparticles. The integrity of the barrier visualised by the green labelled ZO-1 proteins, look similar across the groups.

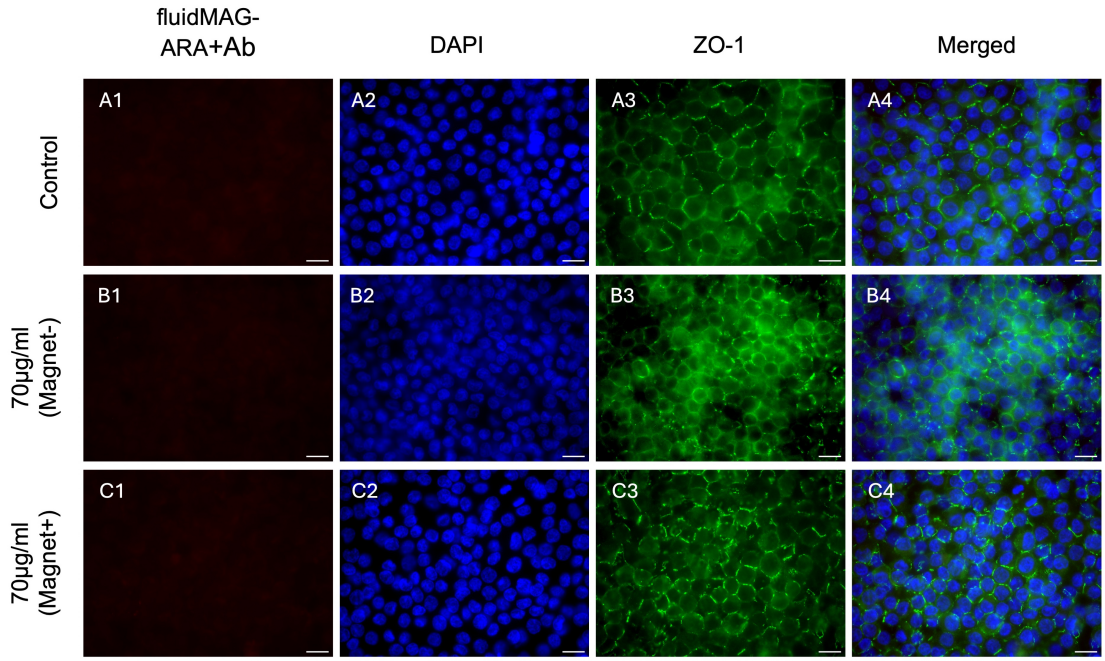

Figure 3.10: Immunofluorescent images of HBMECs uptake of fluidMAG-ARA+Ab Images taken following treatment of a HBMEC mono-culture BBB with 70µg/ml magnet+ (C), 70µg/ml magnet- (B) or no treatment (control)(A). Magnet strength was 0.39T and time on the magnet was ZO-1 (Alexa 488) (green), all nuclei are stained with DAPI (blue) and fluidMAG-ARA+Ab are Goat Anti-Rabbit IgG H&L (Texas Red®). Scale bar = 50nm

These results lead to the testing of fluidMAG-ARA particles, without conjugated antibodies, on the BBB/BBTB models to investigate the transport of these particles. Mean TEER values ±SD results are illustrated in fig3.11 (d.-f.) in a similar manner as results from setup 3. In the 4th setup the MNPs were added at a concentration of 140µg/ml and the magnet treated barriers were placed on a 1.0T magnet for 20 minutes. No disruption of the BBB or BBTB was apparent (P>0.05). Graphs visualising all mean TEER value for both setup 3 and 4 can be found in A figure A.2.

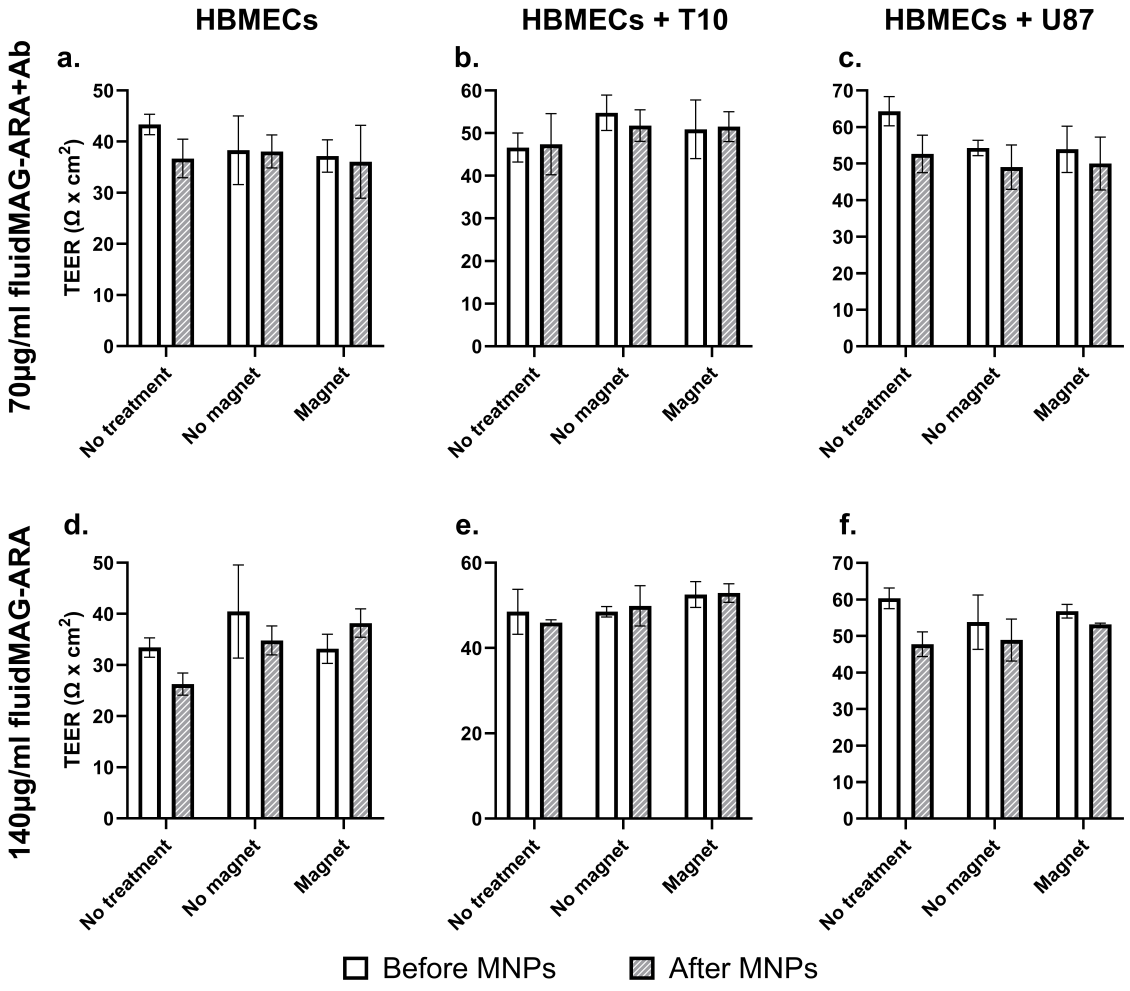

Figure 3.11: Transendothelial Electrical Resistance (TEER) measurements before and after treatment of HBMEC BBB/BBTB Measurements of mean TEER values ±SD displayed in bar charts before (white bars) and after (grey bars) treatment. **a.-c.** 70µg/ml of fluidMAG-ARA+Ab were added on day 5. Magnet group was incubated 5 hours on a 0.39T magnet followed by 19 hours without. **d.-f.** 140µg/ml of fluidMAG-ARA were added on day 6. Magnet group was incubated 20 minutes on a 1.0T magnet followed by 24 hours without. No magnet group was incubated for 24 hours in both experiments.

3.9 Iron concentration of fluidMAG-ARA nanoparticles using Perl's prussian blue stain method

To quantify the iron content in the insert and bottom well for each of the samples from the BBB/BBTB model using fluidMAG-ARA, Pearl's prussian blue method was used. This method was used to develop an assay specifically used for this experiment. The full development process can be found in **??**.

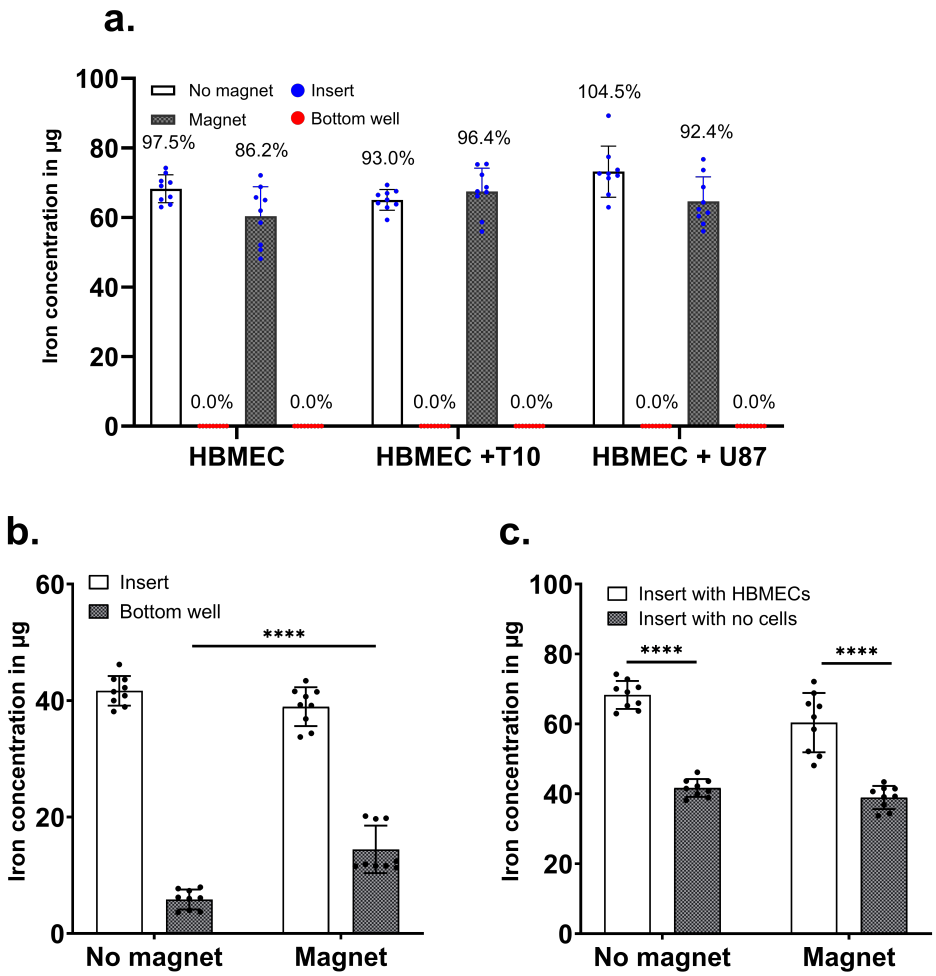

Figure 3.12: Iron concentration for MNP transport across BBB/BBTB. Iron concentration (µg/ml) are presented as mean ± SD. **a.** Iron concentration in medium from inserts and bottom well following BBB/BBTB treatment with 140µg/ml (equal to 70µg per insert) for both magnet and no magnet treatment using a 1.0T magnet for 20 minutes. Above each bar is the mean iron concentration illustrated in percent of 70µg, to illustrate the differences more clearly. **b.** Iron concentration in medium from insert and bottom wells in an insert with no cells for both magnet and no magnet treatment using a 1.0T magnet for 20 minutes. **c.** Difference in iron concentration in medium from insert with HBMECs (a.) and medium from inserts with no cells (b.). An unpaired t-test was used to compare means of iron concentration in the bottom wells (b.) and between medium from inserts with and without cells for both no magnet and magnet treatment (c.) All data was normally distributed.

Cell medium from insert and bottom well were sampled after and analysed using the Perl's prussian blue method. Treated groups were administered 140µg/ml in 500µl medium/insert (equal to 70µg/insert). Mean iron concentrations in the insert from samples on and off a magnet was not significantly different (P>0.05; n=3) ranging from 60.4 ±8.5µg/ml - 73.1±7.3µg/ml. All bottom wells had an iron concentration of 0µg/ml. (figure 3.12 a.). This result lead to testing the transport of MNPs across an insert membrane with no cells seeded on it. This lead to a mean iron concentration of 5.9 ±1.7µg/ml and 14.5±4.1µg/ml for insets off and on a 1T magnet for 20 minutes respectively. The use of a magnet resulted

in a significantly increase in iron concentration in the bottom well (P<0.0001; n=3) (figure 3.12 b.). Finally the difference in iron concentration in the inserts with cells were compared to the iron concentration in the inserts without cells was significant (P<0.0001) (figure 3.12 c.).

Discussion

Delivery of therapeutics across the BBB is an important challenge that is currently being researched extensively but is yet to be solved (Wu et al., 2023). The purpose of this study was to provide a proof-of-concept study of the transport of magnetic nanoparticles across the BBTB. This was done by using an *in vitro* model of the BBTB using a co-culture of either PBECs or HBMECs with T10 cells as the primary model and U87 cells a comparison model and a mono-culture BBB model as a control. This study examined the use of nano-screenMAG-D and fluidMAG-ARA nanoparticles at different concentrations and magnet field strengths with different exposure times.

4.1 Evaluation of the integrity of the blood-brain and blood-brain-tumour barrier model

Good *in vitro* BBB models that mimic the in vivo BBB are essential for studies of drug delivery to the brain, because most drugs are excluded from the brain (Pardridge, 2005). Different cell types can be used to make *in vitro* BBB models based on what is being studied. PBECs might be chosen on the basis of higher TEER values compared to other species like mice or rats. Furthermore, brain tissue, like PBECs, from animal sources are generally easier to obtain, while maintaining many BBB characteristics (M. S. Thomsen et al., 2021). In comparison, HBMECs might be chosen because it, in theory, is a more translational model, especially for the GBM cells utilized in this current study, since they too have human origin. Multiple studies have been made validating both PBECs and HBMECs as good BBB models due to high levels of tight junction proteins Z0-1, claudin-5 and occludin (Eigenmann et al., 2013; Helms et al., 2016). In this current study it was observed that there was a great difference between the integrity of the PBECs and HBMECs BBB model. PBECs in mono-culture reached up to 472 ±65.6 Ω x cm^2 and HBMECs in monoculture reached 43.4 ±2.0Ω x cm^2.
PBECs were initially chosen as the endothelial cells for this study based on their ability to form a tight monolayer. Since the focus of this study is on the drug delivery across the BBTB with T10 cells, it was essential to first observe if T10 cells would impact the BBB with emphasis on the integrity. A pilot study was made to evaluate the optimal timing for treatment, being when the TEER values reach a high and stable value indicating the optimal integrity of the barrier.

TEER values of the PBEC mono-culture reached a max TEER value of 472 ± 65.6 Ω x cm^2 corresponding well with the integrity of similar PBEC BBB models found in other studies (Patabendige et al., 2013; M. S. Thomsen et al., 2021). Constructing a uniform *in vitro* BBB model can be a challenge since factors like temperature changes, handling of the plates during measurements and cellular variance can influence the integrity of the barrier. All

plates were kept in an incubator at 37°C and TEER was measured in a laminar flow bench at room temperature. To account for the difference in temperature during measurements the plates were places on a heating pad set to 37°C. Chopstick electrodes were used for measuring TEER values and all samples were measured in triplicates to account for measurement errors. All samples throughout the project have been handled and measured in the same manner.

The TEER value of the co-culture of PBECs and T10 cells increased significantly more than the mono-culture barrier, which was not according to our expectations. Other studies found that the co-cultures with GBM cells lower the integrity of the barrier (Mendes et al., 2015). Mendes et al. studied the integrity of an *in vitro* BBB model using hCMECs as mono-culture barrierr reaching a maximal TEER value at 32.9 ±7.2 Ωx cm^2 and a co-culture with U87 cells only reaching a maximal TEER value at 18.2 ± 6.7Ωx cm^2 indicating a destructive interference of the U87 (Mendes et al., 2015). Another study by Sanchez et al. similarly observe a decrease in TEER in the co-culture of U87 compared to the mono-culture BBB with either hCMECs or Madin–Darby Canine Kidney Cell line (MDCK) (Sánchez-Dengra et al., 2023). The results of the co-culture BBTB, in this current study, reached a maximum TEER value at 848.6 ±90.0Ωx cm^2 correlating well with TEER values of other co-cultures with either astrocytes, pericytes or both, compared to a mono-culture of PBECs (Helms et al., 2016; M. S. Thomsen et al., 2021). This indicates that the effect that the T10 cells had on the integrity of the barrier is more similar to that of astrocytes or pericytes rather than GBM, at least based on the findings from other studies.

In addition to the PBECs this current study also used HBMECs for establishment of a BBTB model. The TEER values of the HBMECs in this study are rather low compared to other models, like PBEC BBB models. A study by Eigenmann et al. measured a maximal TEER value for HBMECs seeded at 9 x 10^4 cells/cm^2 to 38.9 ±0.928 Ω x cm^2. The mono-culture in this current study reached max TEER values of 43.4 ±2.0Ωx cm^2 and 54.0 ± 4.0Ωx cm^2 and 70.0 ± 1.0Ωx $cm^2$for the co-culture with T10 and U87 respectively. Although the TEER values are lower for HBMECs compared to PBECs, this is not unusual, and the results from this current study regarding TEER values of HBMECs correlates well with other studies (Eigenmann et al., 2013; Helms et al., 2016).

In addition to TEER measurements, an immunocytochemical image of the cells were made. Tight junction proteins claudin 5 and ZO-1 were labelled for the PBEC and HBMEC barriers (figure 3.3) to visualise the integrity and tightness of the barrier. PBECs are larger in size and creates a monolayer of cells contrary to HBMECs that are smaller and forms a multilayer and are much more confluent. It is possible that the multilayer of HBMECs is more incomplete than the monolayer of PBECs which could lead to the lower TEER values. In theory, this could mean a greater passage of MNPs though the HBMEC barrier than the PBEC barrier. Further studies are needed to investigate this speculation further.

4.2 FluidMAG-ARA did not alter the integrity of the BBB/BBTB

The cytotoxic effect of fluidMAG-ARA nanoparticles on HBMECs, T10 and U87 was evaluated *in vitro* by administration of either 0, 35, 70 or 140µg/ml MNPs or DMSO for 24 hours. All cell types showed a significant difference between the DMSO treated cells and all other treatments, as expected. HBMECs were nearly 100% viable for all treatments. In contrast, both U87 and T10 cell showed inconsistent and varying viability for all treatments, even the ones that were not treated. U87 cells did show some significant difference between the different treatment groups. This result confirms the heterogeneity of cancer cells as well as their viability. Cancer cells form spheres, even in culture medium, and the larger the sphere, the more likely it is to contain a necrotic core, as is evident by malignant tumours (Z.-g. Liu & Jiao, 2020). Nevertheless, if the MNPs do have a toxic effect on the cancer cells, it would only prove better for the clinical use of MNPs if used for drug targeting GBM. Other studies also found that MNPs general not are found to exert a cytotoxic effect, but they do show some concentration depended toxicity (Boyer et al., 2010; L. B. Thomsen et al., 2013).

The nano-screenMAG-D nonparticles were administered to a BBTB with PBECs and T10 cells or U87 and to a mono-culture BBB model at a concentration of 70µg/ml. The same particles were used by Thomsen et al. who observed that the particles passed through the BBB model with HBMECs under the influence of an external 0.39T magnet (L. B. Thomsen et al., 2013). While using the same particles in this current study, a toxic effect to the cells was observed and the integrity of the barriers decreased significantly as evident by a drop in TEER ($P<0.0001$; $n=3$) for all barriers treated with nano-screenMAG-D. The sudden toxicity of these particles could be due to the particles being expired. As earlier explained, this result lead to the purchase of the fluidMAG-ARA nanoparticles. These new particles coated with glucoronic acid to ensure better biocompatibility for in vivo use. The particles were not fluorescent and were therefore conjugated with fluorescent antibodies for visualisation and quantifying purposes in a similar manner as Thomsen et al. (L. B. Thomsen et al., 2013). To confirm successful conjugation of the antibodies the MNPs were tested by fluorescence microscopy in order to visualise the particles. Based on the fluorescent images as presented in section 3.4, it is clear to visualise the antibodies in the sample compared to the fluidMAG-ARA without antibodies indicating a successful conjugation of the antibodies. It would have been preferable to examine the exact amount of bound antibodies to the MNPs. This could be done by measuring the fluorescence of a sample of the MNPs compared to the fluorescence of the supernatant and subtracting this value from the fluorescence of the initial MNPs with antibodies (Tam et al., 2017). For further studies of the particles transmission electron microscop (TEM) imaging can be used to visualise the exact construct and size of the particles (Zhang & Wang, 2023).

FluidMAG-ARA nanoparticles were measured to a mean hydrodynamic size of 105.4 ±2.427nm and fluidMAG-ARA+Ab to 263.5 ±23.97nm with a PDI of 0.243 ±0.0207 and 0.611 ±0.0294 respectively. Looking at the size graph illustrated in figure 3.6 it is evi-

dent that the intensity is much higher and the size span is much lower compared to the fluidMAG-ARA+Ab. A small spike is visible on the size graph for both particles, which is most likely some insignificant measurement error from the machine. The size difference clearly indicates a difference in size also indicating that antibodies have been successfully conjugated to the particles. PDI is used to estimate the average uniformity of a particle solution, the larger the PDI value is. A large PDI value could indicate a larger size distribution, but also indicate particle aggregation throughout the sample (Hughes et al., 2015). FluidMAG-ARA+Ab has a lager size distribution based on the SD of 23.97nm compared to 2.427nm for the naked fluidMAG-ARA. Together with a higher PDI of the fludMAG-ARA+AB it is either an indication of particle aggregation or differences in the concentration of antibodies conjugated to each particle. Furthermore, thee magnetic properties of the particles are visualise, and it is clear to see the formation of the MNPs when influenced by an external magnet (see figure 3.6).

The zeta potential of nanoparticles reflects the electrical potential and slipping plane of the particle. The zeta potential of the fluidMAG-ARA was slightly more negative (35.35 ±1.845mV) than for fludMAG-ARA+Ab (-22.26 ±1-043mV). A negative zeta potential increases the plasma circulation because it attracts less protein adsorption (Boyer et al., 2010). Negatively charged particles are repelled by the negatively charged surface of the endothelial cells causing them to stay longer in circulation (Krüger-Genge et al., 2019). A study by Kedzierske et al. indicates that a suspension with a zeta potential of higher than +30mV or lower than -30mV shows good stability for the sample (Kedzierska et al., 2021). Based on this it can be suggested that fluidMAG-ARA nanoparticles, without antibodies, might be a better in vivo candidate than the ones conjugated with antibodies.

The aim of the initial setup using fludMAG-ARA+Ab was to evaluate the optimal concentration of MNPs that could cross the BBTB and simultaneously cause the least damage to the barrier. Thomsen et al. conducted a similar setup using different concentrations of MNPs (35, 70 and 140µg/ml) (L. B. Thomsen et al., 2013). The results of this current study clearly indicates that none of the concentrations did have any destructive effect on the barriers, based on the TEER values before and after treatment. Conversely all treatment groups seemed to show an increase in TEER (see figure 3.8. This setup was made with a HBMEC monoculture BBB model and 30 minutes exposure of a 0.39T magnet. The increase in TEER could indicate a defence mechanism in the endothelial cells in response to the added nanoparticles. Although, this does not seem to be a trend in the other HBMEC BBB transport setups analysed in this study. From the analysis using the fluorescent microscopy, no particles were visible in the medium from the bottom well, only in the media from the inserts (figure 3.9 Thomsen et al. found a positive linear correlation between dose and response for inserts with cells subjected to a magnetic field of 0.39T for 5 hours, but they found almost no transport of MNPs in inserts with cells and no magnetic subjection and in inserts with no cells and magnetic subjection (L. B. Thomsen et al., 2013).

4.3 Evaluation of the transport of magnetic nanoparticles across the BBB/BBTB

This current study aimed to transport magnetic nanoparticles across an *in vitro* BBB model. The use of a 0.39T magnet did not make a difference from the 1.0T magnet in the effectiveness of transporting MNPs across the BBB. The first setup was made with a 0.39T magnet applied for 30 minutes to a sample plate. A similar setup was made by Chertok et al. using starch coated superparamagnetic iron oxide nanoparticles (SPIONs) (110nm) targeted towards a rat brain tumour in vivo. Quantified by MRI Cherrtok et al. found a 5-fold increase in nanoparticle accumulation in the tumour for the magnetic targeted nanoparticles (Chertok et al., 2008). Since this current study did not find any transport of nanoparticles crossing the barrier *in vitro*, the exposure time of the magnet was increased. The study mentioned earlier by Thomsen et al. investigated the transport of SPIONs through HBMECs using a 0.39T magnet for 5 hours, resulting in an 8-fold increase in particles transported across the barrier with a concentration at 70µg/ml (L. B. Thomsen et al., 2013). Based on this, the duration time of the magnet was changed from 30 minutes to 5 hours. Still no particles were observed to pass through the barrier. The HBMECs from the inserts were also analysed for uptake of fluidMAG-ARA+Ab. Both the HBMECs with and without magnetic subjection did not show any indications of uptake of the particles compared to the control. The endothelial cells were labelled with ZO-1 and did not show any changes compared to the control. Thomsen et al. did find that when brain capillary endothelial cells were subjected to 140µg of MNPs that they appear inside the cells. Gkountas et al. provides a model for correlation between the magnetic field strength and the percentage of MNPs passing through the BBB showing a higher passing percentage of MNPs with a stronger magnetic field (Gkountas et al., 2021). Hereby the magnetic strength was increased to 1.0T, still without observing any particles passing the barrier.

Based on the analysis made in this current study the *in vitro* transport studies all proved that either of the magnetic nanoparticles used were able to pass the cell layer in the transwell inserts. There was no seemingly difference between the magnet treated and no magnet treated plates for either the BBB or BBTB models with regards to transport of MNPs. However, whether the fluidMAG-ARA particles are capable of passing through the BBTB is still inconclusive since many studies proves the transport of MNPs over the BBB (Betzer et al., 2017; Chen et al., 2022; Ivask et al., 2018; L. B. Thomsen et al., 2013). At first we speculated if the bond between the antibodies and the fludMAG-ARA particles was so weak that when influenced by the magnet the particles would be pulled from the antibodies through the endothelial cells. Later analysis using Perl's prussian blue staining confirmed that the iron content in the medium on the transluminal side was not measurable. Although the iron content in the bottom wells were not detectable, the detected iron content in the inserts of HBMEC mono-culture + magnet seems to be lower than in the inserts with BBTB co-culture with T10 or U87. This could potentially be an indication of some transport of across the HBMEC barrier compared to the co-culture barrier indicating that GBM cells strengthens the barrier as also evident by the TEER values. Further studies

are needed to confirm these speculations. Moreover, using Perl's prussian blue analysis it was clear that the fluidMAG-ARA particles were able to cross the insert membrane with no cells. This result correlated with expected results of more nanoparticles passing under the influence of a magnet compared to no magnet (Ramaswamy et al., 2015).

Ramaswamy et al.studied how a magnetic field influences the motion of magnetic nanoparticles (274.6 ± 40 nm) in rat brain tissue. They used an either high (0.1T) or low (0.02T) uniform magnetic field with an either high or low MNP concentration. The study found a direct correlation between the size of the magnetic field and the chaining formation of the MNPs. Because of the suparperimagnetic effect of the MNPs the all have a slightly induced magnetic field that will overlap one another during magnetic stimulation. This causes the MNPs to attract one another an form chains. After 10 minutes with the highest concentration and magnetic field the chain formation length was measured at 12.51 ± 3.5µm (Ramaswamy et al., 2015). Considering the size of the magnetic field used in this study, it is very likely that the MNPs used could form some form of chaining thereby making them less able to pass through the endothelial cells.
To design a nanoparticle with a good biodistribution following intravenous injection there are some key things to consider. Patel et al. defines size of <100nm as one of the key aspects for an optimal nanoparticle to enter the CNS. It is believed that particles larger will have difficulty passing through the extracellular space in the brain (Patel et al., 2012). Most studies for drug delivery to the brain uses nanoparticles with a size between 10nm-100nm (Saraiva et al., 2016). As a general rule studies have found higher permeability through the BBB as the nanoparticles decrease in size (Kulkarni & Feng, 2013). The nanoparticles used in this current study are both >100nm, which also might reduce the likelihood of non-targeted transport. The proptimal size of the nanoparticle might be lower than used in this current study. Betzer et al. studied the optimal size for Insulin-gold-nanparticles to cross the BBB to be around 20nm for BBB transcytosis (Betzer et al., 2017).

Surface functionalisation is another important aspect to consider for optimising passage of MNPs through the BBB in vivo. Polymers, especially polyethylene glycol (PEG) are commonly used for coating nanoparticles to increase the circulation time by preventing opsonization and thereby making the particles available for longer to interact with the epithelial cells (Suk et al., 2016). Several studies use PEGylated magnetic nanoparticles for in vivo passage of the BBB (Chen et al., 2022; Ding et al., 2014; Ivask et al., 2018; Qiao et al., 2012). Other studies used silica (SiO_2) (Li et al., 2022; X. Zhao et al., 2016) or gold (Au) (Betzer et al., 2017; Chen et al., 2022) as coating MNPs for more optimal delivery. In addition to using some form of coating, another valid method for delivery of MNPs ins by encapsulating them in liposomes (Ding et al., 2014; L. B. Thomsen et al., 2019; M. Zhao et al., 2012).

Targeting the MNPs to specific receptors on the BBB by adding specific proteins or ligands can help improve the uptake and transcytosis. One of the most studied of such receptors on the BBB is the transferrin receptor (TfR) (Georgieva et al., 2014). Ding et al. studied the transport of TfR targeted PEGylated magnetic liposomes across an *in vitro* HBMEC co-

cultre BBB model with human astrocytes under the influence of a magnetic field compared to none. Ding et al. found that approximately 50% of TfR embedded magnetic liposomes under magnetic force passed the BBB both at 6, 12 and 24 hours. At 24 hours it was also evident that the percent passage of TfR embedded magnetic liposomes absent of a magnetic field was higher than magnetic liposomes under the influence of a magnetic field (Ding et al., 2014). This indicates that the most effective method for drug delivery to the brain is through a combination of targeted MNPs under influence of a magnetic field. A study by Chen et al. confirms that the increase in transport across the BBB using a targeted MNP is more efficient than just naked MNPs. In their study they used SPOINs coated in gold and functionalised by PEGylation (SPOI-Au-PEG) and found that they did accumulate in the brain slightly more under a static magnetic field compared to none. Later they conjugated the SPOI-Au-PEG with insulin to facilitate BBB crossing by receptor-mediated transcytosis. This significantly improved passage across the BBB. Finally the study showed that the greatest potential for transport was using the insulin conjugated SPOI-Au-PEG under the influence of a static magnetic field (Chen et al., 2022).

Although no seemingly transport of MNPs across the BBB and BBTB was found in this study, the particles still posses great potential for transport of conjugated to the right peptide. Magnetic nanoparticles are excellent for drug delivery even despite their magnetic potential. A study by Dilnawaz et al. studied magnetic nanoparrticles for drug delivery due to their ability to be easily engineered to have a high drug load capacity and good biocompatibility (Dilnawaz et al., 2012). Li et al. studied a new idea for treatment of GBM by ferroptosis hereby illustrating the potential of using MNPs in drug delivery to the brain. Li et al. have designed a vehicle for drug therapeutics using small interfering RNA encapsulated in exosomes conjugated to silica coated magnetic nanoparticles. Furthermore the exosomes were targeted using angiopeptin-2 which is a potent ligand for LRP1, which is upregulated on brain endothelial cells and some GBM cells. Not only did they show success in delivering this conjugated system to the brain under magnetic stimulation, but they also found that naked MNPs did not significantly accumulate in the brain (Li et al., 2022).

T10 cells were used to model GBM forming an *in vitro* co-culture BBTB. The TfR has been studied extensively for drug delivery across the BBB also for the targeting of MNPs (Ding et al., 2014; L. B. Thomsen et al., 2019). LRP1 is another potent target, which is highly expressed on brain endothelial cells and glioma cells, making this an optimal target for drug delivery because it both secure passage over the BBB as well as targeting of the tumour cells (Jiang et al., 2018). The LRP1 ligand angiopep-2 is thought to induce receptor mediated transcytosis and has been targeted with success in other studies (di Polidoro et al., 2022; Li et al., 2022). From the RT-qPCR analysis of the T10 cells in this current study, the relative gene expression of LRP1 was significantly lower compared to U87. To evaluate the actual LRP1 protein expressed on the T10 cells analysis like Western blotting (Mahmood & Yang, 2012) or flow cytometry (Hogg et al., 2015) could be used. Furthermore, the RT-qPCR analysis of the relative gene expression illustrates the homogeneity of cancer cells

and a distinct genetic difference between tumour cell lines.

4.4 Optimisation of methods and future perspectives

It is unclear exactly why the MNPs did not pass through the endothelial cells in either of the barriers. Future experiments should be made to clarify why the particles did not pass as proved by other studies. One way to do this would be to measure the hydrodynamic size before and after a 24 hour incubation at 37°C to MNPs to check for aggregations. Another area of improvement is the analysis of the particles transported through thee barraier. The Perls prussian blue method did pose some inconsistency and needs to be tested more to truly validate the method for measuring the exact concentration of the iron content of the medium.

Most studies done with MNPs have been made on a healthy BBB and proved successful passage of the particles using an external magnet. More knowledge of a good BBTB *in vitro* model for GBM is needed. U87 has been used as the gold standard for GBM studies (Boccellato & Rehm, 2022), but because of the heterogeneity of GBM tumours it would be beneficial to establish a variety of GBM *in vitro* models. To optimise the BBTB *in vitro* model it would be a better comparison to compare a co-cultre BBTB with HBMECs and T10 with a control culture HBMEC and human astrocyte (HA) barrier. It would also be interesting to see the effect of GBM cells together with HAs or to seed the GBM cells longer time in advance than just one day.

Finally, it would be relevant to compare naked MNPs, as used in this current study, to some targeted MNPs to better evaluate the potential of their passage through the BBTB. Most of the literature, as presented, tend to conclude that the most effective way to transport MNPs across the BBB is with a combination of both specific targeting as well as magnetic field influence. It would be interesting to see a study comparing the two types of MNPs in a BBTB model.

Conclusion

The objective of this study was to evaluate the transport of MNPs through the BBTB with T10 cells. However, this study did not find that fluidMAG-ARA nanoparticles were able to pass through an *in vitro* BBTB or BBB model *in vitro* at different concentration, or under subjection of an external magnetic field. These findings are contrary to the initial hypothesis. Nevertheless, it was evident that fluidMAG-ARA were non-toxic to the endothelial cells, and did not alter the integrity of either the BBB or BBTB models. Therefore, the potential of using MNPs for drug delivery across the BBTB remains. Furthermore, the integrity of the BBB and the BBTB using either T10 or U87 cells, did seem to differ slightly with a tendency of a higher TEER value for the BBTB models in general. The findings of this study indicates a need for specific targeting of fluidMAG-ARA to endothelial cells and GBM cells to facilitate greater passage of the BBTB. This may constitute the object of future studies.

Bibliography

Abbott, N. J., Patabendige, A. A., Dolman, D. E., Yusof, S. R., & Begley, D. J. (2010). Structure and function of the blood–brain barrier. *Neurobiology of disease*, *37*(1), 13–25.

Abbott, N. J., Rönnbäck, L., & Hansson, E. (2006). Astrocyte–endothelial interactions at the blood–brain barrier. *Nature reviews neuroscience*, *7*(1), 41–53.

Ahir, B. K., Engelhard, H. H., & Lakka, S. S. (2020). Tumor development and angiogenesis in adult brain tumor: Glioblastoma. *Molecular neurobiology*, *57*, 2461–2478.

Allafchian, A., & Hosseini, S. S. (2019). Antibacterial magnetic nanoparticles for therapeutics: A review. *IET nanobiotechnology*, *13*(8), 786–799.

Angom, R. S., Nakka, N. M. R., & Bhattacharya, S. (2023). Advances in glioblastoma therapy: An update on current approaches. *Brain sciences*, *13*(11), 1536.

Anjum, K., Shagufta, B. I., Abbas, S. Q., Patel, S., Khan, I., Shah, S. A. A., Akhter, N., & ul Hassan, S. S. (2017). Current status and future therapeutic perspectives of glioblastoma multiforme (gbm) therapy: A review. *Biomedicine & Pharmacotherapy*, *92*, 681–689.

Arvanitis, C. D., Ferraro, G. B., & Jain, R. K. (2020). The blood–brain barrier and blood–tumour barrier in brain tumours and metastases. *Nature Reviews Cancer*, *20*(1), 26–41.

Betzer, O., Shilo, M., Opochinsky, R., Barnoy, E., Motiei, M., Okun, E., Yadid, G., & Popovtzer, R. (2017). The effect of nanoparticle size on the ability to cross the blood–brain barrier: An in vivo study. *Nanomedicine*, *12*(13), 1533–1546.

Billotey, C., Wilhelm, C., Devaud, M., Bacri, J., Bittoun, J., & Gazeau, F. (2003). Cell internalization of anionic maghemite nanoparticles: Quantitative effect on magnetic resonance imaging. *Magnetic Resonance in Medicine: An Official Journal of the International Society for Magnetic Resonance in Medicine*, *49*(4), 646–654.

Boccellato, C., & Rehm, M. (2022). Glioblastoma, from disease understanding towards optimal cell-based in vitro models. *Cellular Oncology*, *45*(4), 527–541.

Boutry, S., Forge, D., Burtea, C., Mahieu, I., Murariu, O., Laurent, S., Vander Elst, L., & Muller, R. N. (2009). How to quantify iron in an aqueous or biological matrix: A technical note. *Contrast media & molecular imaging*, *4*(6), 299–304.

Boyer, C., Whittaker, M. R., Bulmus, V., Liu, J., & Davis, T. P. (2010). The design and utility of polymer-stabilized iron-oxide nanoparticles for nanomedicine applications. *NPG Asia Materials*, *2*(1), 23–30.

Busquets, M. A., Espargaró, A., Sabaté, R., & Estelrich, J. (2015). Magnetic nanoparticles cross the blood-brain barrier: When physics rises to a challenge. *Nanomaterials*, *5*(4), 2231–2248.

Chen, J., Yuan, M., Madison, C. A., Eitan, S., & Wang, Y. (2022). Blood-brain barrier crossing using magnetic stimulated nanoparticles. *Journal of Controlled Release*, *345*, 557–571.

Cheng, X., Xie, Q., & Sun, Y. (2023). Advances in nanomaterial-based targeted drug delivery systems. *Frontiers in bioengineering and biotechnology*, *11*, 1177151.

Chertok, B., Moffat, B. A., David, A. E., Yu, F., Bergemann, C., Ross, B. D., & Yang, V. C. (2008). Iron oxide nanoparticles as a drug delivery vehicle for mri monitored magnetic targeting of brain tumors. *Biomaterials*, *29*(4), 487–496.

Denizot, B., Tanguy, G., Hindre, F., Rump, E., Le Jeune, J. J., & Jallet, P. (1999). Phosphorylcholine coating of iron oxide nanoparticles. *Journal of Colloid and Interface Science*, *209*(1), 66–71.

di Polidoro, A. C., Cafarchio, A., Vecchione, D., Donato, P., De Nola, F., & Torino, E. (2022). Revealing angiopep-2/lrp1 molecular interaction for optimal delivery to glioblastoma (gbm). *Molecules*, *27*(19), 6696.

Dilnawaz, F., Singh, A., Mewar, S., Sharma, U., Jagannathan, N., & Sahoo, S. K. (2012). The transport of non-surfactant based paclitaxel loaded magnetic nanoparticles across the blood brain barrier in a rat model. *Biomaterials*, *33*(10), 2936–2951.

Ding, H., Sagar, V., Agudelo, M., Pilakka-Kanthikeel, S., Atluri, V. S. R., Raymond, A., Samikkannu, T., & Nair, M. P. (2014). Enhanced blood–brain barrier transmigration using a novel transferrin embedded fluorescent magneto-liposome nanoformulation. *Nanotechnology*, *25*(5), 055101.

Dolgin, E. (2016). Venerable brain-cancer cell line faces identity crisis. *Nature*, *537*(7619).

Eigenmann, D. E., Xue, G., Kim, K. S., Moses, A. V., Hamburger, M., & Oufir, M. (2013). Comparative study of four immortalized human brain capillary endothelial cell lines, hcmec/d3, hbmec, ty10, and bb19, and optimization of culture conditions, for an in vitro blood–brain barrier model for drug permeability studies. *Fluids and Barriers of the CNS*, *10*, 1–17.

Erices, J. I., Bizama, C., Niechi, I., Uribe, D., Rosales, A., Fabres, K., Navarro-Martínez, G., Torres, Á., San Martín, R., Roa, J. C., et al. (2023). Glioblastoma microenvironment and invasiveness: New insights and therapeutic targets. *International journal of molecular sciences*, *24*(8), 7047.

Esemen, Y., Awan, M., Parwez, R., Baig, A., Rahman, S., Masala, I., Franchini, S., & Giakoumettis, D. (2022). Molecular pathogenesis of glioblastoma in adults and future perspectives: A systematic review. *International Journal of Molecular Sciences*, *23*(5), 2607.

Farzin, A., Etesami, S. A., Quint, J., Memic, A., & Tamayol, A. (2020). Magnetic nanoparticles in cancer therapy and diagnosis. *Advanced healthcare materials*, *9*(9), 1901058.

Flores-Rojas, G. G., López-Saucedo, F., Vera-Graziano, R., Mendizabal, E., & Bucio, E. (2022). Magnetic nanoparticles for medical applications: Updated review. *Macromol*, *2*(3), 374–390.

Fortin, J.-P., Gazeau, F., & Wilhelm, C. (2008). Intracellular heating of living cells through néel relaxation of magnetic nanoparticles. *European Biophysics Journal*, *37*, 223–228.

Freeman, M., Arrott, A., & Watson, J. (1960). Magnetism in medicine. *Journal of Applied Physics*, *31*(5), S404–S405.

Fu, B. M. (2018). Transport across the blood-brain barrier. *Molecular, Cellular, and Tissue Engineering of the Vascular System*, 235–259.

Gallego, O. (2015). Nonsurgical treatment of recurrent glioblastoma. *Current oncology*, *22*(4), 273–281.

Gawdi, R., & Emmady, P. (2020). Physiology, blood brain barrier. *StatPearls*.

Georgieva, J. V., Hoekstra, D., & Zuhorn, I. S. (2014). Smuggling drugs into the brain: An overview of ligands targeting transcytosis for drug delivery across the blood–brain barrier. *Pharmaceutics*, *6*(4), 557–583.

Gkountas, A. A., Polychronopoulos, N. D., Sofiadis, G. N., Karvelas, E. G., Spyrou, L. A., & Sarris, I. E. (2021). Simulation of magnetic nanoparticles crossing through a simplified blood-brain barrier model for glioblastoma multiforme treatment. *Computer Methods and Programs in Biomedicine*, *212*, 106477.

Goodwin, S., Peterson, C., Hoh, C., & Bittner, C. (1999). Targeting and retention of magnetic targeted carriers (mtcs) enhancing intra-arterial chemotherapy. *Journal of magnetism and magnetic materials*, *194*(1-3), 132–139.

Greiffenberg, L., Goebel, W., Kim, K. S., Weiglein, I., Bubert, A., Engelbrecht, F., Stins, M., & Kuhn, M. (1998). Interaction of listeria monocytogenes with human brain microvascular endothelial cells: Inlb-dependent invasion, long-term intracellular growth, and spread from macrophages to endothelial cells. *Infection and immunity*, *66*(11), 5260–5267.

Hamilton, S. R., Liu, B., Parsons, R. E., Papadopoulos, N., Jen, J., Powell, S. M., Krush, A. J., Berk, T., Cohen, Z., Tetu, B., et al. (1995). The molecular basis of turcot's syndrome. *New England Journal of Medicine*, *332*(13), 839–847.

Hansen, S., Rasmussen, B. K., Laursen, R. J., Kosteljanetz, M., Schultz, H., Nørgård, B. M., Guldberg, R., & Gradel, K. O. (2018). Treatment and survival of glioblastoma patients in denmark: The danish neuro-oncology registry 2009–2014. *Journal of neuro-oncology*, *139*, 479–489.

Helms, H. C., Abbott, N. J., Burek, M., Cecchelli, R., Couraud, P.-O., Deli, M. A., Förster, C., Galla, H. J., Romero, I. A., Shusta, E. V., et al. (2016). In vitro models of the blood–brain barrier: An overview of commonly used brain endothelial cell culture models and guidelines for their use. *Journal of Cerebral Blood Flow & Metabolism*, *36*(5), 862–890.

Högemann, D., Ntziachristos, V., Josephson, L., & Weissleder, R. (2002). High throughput magnetic resonance imaging for evaluating targeted nanoparticle probes. *Bioconjugate Chemistry*, *13*(1), 116–121.

Hogg, K., Thomas, J., Ashford, D., Cartwright, J., Coldwell, R., Weston, D. J., Pillmoor, J., Surry, D., & O'Toole, P. (2015). Quantification of proteins by flow cytometry: Quantification of human hepatic transporter p-gp and oatp1b1 using flow cytometry and mass spectrometry. *Methods*, *82*, 38–46.

Hosu, O., Tertis, M., & Cristea, C. (2019). Implication of magnetic nanoparticles in cancer detection, screening and treatment. *Magnetochemistry*, *5*(4), 55.

Hughes, J. M., Budd, P. M., Grieve, A., Dutta, P., Tiede, K., & Lewis, J. (2015). Highly monodisperse, lanthanide-containing polystyrene nanoparticles as potential standard reference materials for environmental "nano" fate analysis. *Journal of Applied Polymer Science*, *132*(24).

Ivask, A., Pilkington, E. H., Blin, T., Käkinen, A., Vija, H., Visnapuu, M., Quinn, J. F., Whittaker, M. R., Qiao, R., Davis, T. P., et al. (2018). Uptake and transcytosis of

functionalized superparamagnetic iron oxide nanoparticles in an in vitro blood brain barrier model. *Biomaterials science*, *6*(2), 314–323.

Jiang, Y., Yang, W., Zhang, J., Meng, F., & Zhong, Z. (2018). Protein toxin chaperoned by lrp-1-targeted virus-mimicking vesicles induces high-efficiency glioblastoma therapy in vivo. *Advanced Materials*, *30*(30), 1800316.

Jiao, H., Wang, Z., Liu, Y., Wang, P., & Xue, Y. (2011). Specific role of tight junction proteins claudin-5, occludin, and zo-1 of the blood–brain barrier in a focal cerebral ischemic insult. *Journal of Molecular Neuroscience*, *44*, 130–139.

Kanderi, T., & Gupta, V. (2022). Glioblastoma multiforme. In *Statpearls [internet]*. StatPearls Publishing.

Kedzierska, M., Potemski, P., Drabczyk, A., Kudlacik-Kramarczyk, S., Glab, M., Grabowska, B., Mierzwinski, D., & Tyliszczak, B. (2021). The synthesis methodology of pegylated fe3o4@ ag nanoparticles supported by their physicochemical evaluation. *Molecules*, *26*(6).

Kędzierska, M., Potemski, P., Drabczyk, A., Kudłacik-Kramarczyk, S., Głąb, M., Grabowska, B., Mierzwiński, D., & Tyliszczak, B. (2021). The synthesis methodology of pegylated fe3o4@ ag nanoparticles supported by their physicochemical evaluation. *Molecules*, *26*(6), 1744.

Kong, S. D., Lee, J., Ramachandran, S., Eliceiri, B. P., Shubayev, V. I., Lal, R., & Jin, S. (2012). Magnetic targeting of nanoparticles across the intact blood–brain barrier. *Journal of controlled release*, *164*(1), 49–57.

Krex, D., Klink, B., Hartmann, C., Von Deimling, A., Pietsch, T., Simon, M., Sabel, M., Steinbach, J. P., Heese, O., Reifenberger, G., et al. (2007). Long-term survival with glioblastoma multiforme. *Brain*, *130*(10), 2596–2606.

Krüger-Genge, A., Blocki, A., Franke, R.-P., & Jung, F. (2019). Vascular endothelial cell biology: An update. *International journal of molecular sciences*, *20*(18), 4411.

Kugler, E. C., Greenwood, J., & MacDonald, R. B. (2021). The "neuro-glial-vascular" unit: The role of glia in neurovascular unit formation and dysfunction. *Frontiers in Cell and Developmental Biology*, *9*, 732820.

Kulkarni, S. A., & Feng, S.-S. (2013). Effects of particle size and surface modification on cellular uptake and biodistribution of polymeric nanoparticles for drug delivery. *Pharmaceutical research*, *30*, 2512–2522.

Kumar, A., Jena, P. K., Behera, S., Lockey, R. F., Mohapatra, S., & Mohapatra, S. (2010). Multifunctional magnetic nanoparticles for targeted delivery. *Nanomedicine: Nanotechnology, Biology and Medicine*, *6*(1), 64–69.

Lathia, J. D., Mack, S. C., Mulkearns-Hubert, E. E., Valentim, C. L., & Rich, J. N. (2015). Cancer stem cells in glioblastoma. *Genes & development*, *29*(12), 1203–1217.

Lee, M., & Jayant, R. (2019). Penetration of the blood-brain barrier by peripheral neuropeptides: New approaches to enhancing transport and endogenous expression. *Cell and tissue research*, *375*, 287–293.

Li, B., Chen, X., Qiu, W., Zhao, R., Duan, J., Zhang, S., Pan, Z., Zhao, S., Guo, Q., Qi, Y., et al. (2022). Synchronous disintegration of ferroptosis defense axis via engi-

neered exosome-conjugated magnetic nanoparticles for glioblastoma therapy. *Advanced Science*, *9*(17), 2105451.

Lim, E.-K., Jang, E., Lee, K., Haam, S., & Huh, Y.-M. (2013). Delivery of cancer therapeutics using nanotechnology. *Pharmaceutics*, *5*(2), 294–317.

Liu, W.-Y., Wang, Z.-B., Zhang, L.-C., Wei, X., & Li, L. (2012). Tight junction in blood-brain barrier: An overview of structure, regulation, and regulator substances. *CNS neuroscience & therapeutics*, *18*(8), 609–615.

Liu, Z.-g., & Jiao, D. (2020). Necroptosis, tumor necrosis and tumorigenesis. *Cell stress*, *4*(1), 1.

Löscher, W., & Potschka, H. (2005). Blood-brain barrier active efflux transporters: Atp-binding cassette gene family. *NeuroRx*, *2*(1), 86–98.

Louis, D. N., Perry, A., Wesseling, P., Brat, D. J., Cree, I. A., Figarella-Branger, D., Hawkins, C., Ng, H., Pfister, S. M., Reifenberger, G., et al. (2021). The 2021 who classification of tumors of the central nervous system: A summary. *Neuro-oncology*, *23*(8), 1231–1251.

Luissint, A.-C., Artus, C., Glacial, F., Ganeshamoorthy, K., & Couraud, P.-O. (2012). Tight junctions at the blood brain barrier: Physiological architecture and disease-associated dysregulation. *Fluids and Barriers of the CNS*, *9*, 1–12.

Maeda, H., Wu, J., Sawa, T., Matsumura, Y., & Hori, K. (2000). Tumor vascular permeability and the epr effect in macromolecular therapeutics: A review. *Journal of controlled release*, *65*(1-2), 271–284.

Mahmood, T., & Yang, P.-C. (2012). Western blot: Technique, theory, and trouble shooting. *North American journal of medical sciences*, *4*(9), 429.

Martinez-Lage, M., Lynch, T. M., Bi, Y., Cocito, C., Way, G. P., Pal, S., Haller, J., Yan, R. E., Ziober, A., Nguyen, A., et al. (2019). Immune landscapes associated with different glioblastoma molecular subtypes. *Acta neuropathologica communications*, *7*, 1–12.

Materón, E. M., Miyazaki, C. M., Carr, O., Joshi, N., Picciani, P. H., Dalmaschio, C. J., Davis, F., & Shimizu, F. M. (2021). Magnetic nanoparticles in biomedical applications: A review. *Applied Surface Science Advances*, *6*, 100163.

Mbeunkui, F., & Johann, D. J. (2009). Cancer and the tumor microenvironment: A review of an essential relationship. *Cancer chemotherapy and pharmacology*, *63*, 571–582.

Mendes, B., Marques, C., Carvalho, I., Costa, P., Martins, S., Ferreira, D., & Sarmento, B. (2015). Influence of glioma cells on a new co-culture in vitro blood–brain barrier model for characterization and validation of permeability. *International Journal of Pharmaceutics*, *490*(1-2), 94–101.

Moroz, P., Jones, S., & Gray, B. (2002). Magnetically mediated hyperthermia: Current status and future directions. *International Journal of Hyperthermia*, *18*(4), 267–284.

Oldendorf, W. H., Cornford, M. E., & Brown, W. J. (1977). The large apparent work capability of the blood-brain barrier: A study of the mitochondrial content of capillary endothelial cells in brain and other tissues of the rat. *Annals of Neurology: Official Journal of the American Neurological Association and the Child Neurology Society*, *1*(5), 409–417.

Pardridge, W. M. (2005). The blood-brain barrier: Bottleneck in brain drug development. *NeuroRx*, *2*, 3–14.

Patabendige, A., Skinner, R. A., & Abbott, N. J. (2013). Establishment of a simplified in vitro porcine blood–brain barrier model with high transendothelial electrical resistance. *Brain research*, *1521*, 1–15.

Patel, T., Zhou, J., Piepmeier, J. M., & Saltzman, W. M. (2012). Polymeric nanoparticles for drug delivery to the central nervous system. *Advanced drug delivery reviews*, *64*(7), 701–705.

Petzold, G. C., & Murthy, V. N. (2011). Role of astrocytes in neurovascular coupling. *Neuron*, *71*(5), 782–797.

Pfaffl, M. W. (2001). A new mathematical model for relative quantification in real-time rt–pcr. *Nucleic acids research*, *29*(9), e45–e45.

Price, M., Neff, C., Nagarajan, N., Kruchko, C., Waite, K. A., Cioffi, G., Cordeiro, B. B., Willmarth, N., Penas-Prado, M., Gilbert, M. R., et al. (2024). Cbtrus statistical report: American brain tumor association & nci neuro-oncology branch adolescent and young adult primary brain and other central nervous system tumors diagnosed in the united states in 2016–2020. *Neuro-oncology*, *26*(Supplement_3), iii1–iii53.

Pulgar, V. M. (2019). Transcytosis to cross the blood brain barrier, new advancements and challenges. *Frontiers in neuroscience*, *12*, 1019.

Qiao, R., Jia, Q., Huwel, S., Xia, R., Liu, T., Gao, F., Galla, H.-J., & Gao, M. (2012). Receptor-mediated delivery of magnetic nanoparticles across the blood–brain barrier. *ACS nano*, *6*(4), 3304–3310.

Ramaswamy, B., Kulkarni, S. D., Villar, P. S., Smith, R. S., Eberly, C., Araneda, R. C., Depireux, D. A., & Shapiro, B. (2015). Movement of magnetic nanoparticles in brain tissue: Mechanisms and impact on normal neuronal function. *Nanomedicine: Nanotechnology, Biology and Medicine*, *11*(7), 1821–1829.

Rathi, S., Griffith, J. I., Zhang, W., Zhang, W., Oh, J.-H., Talele, S., Sarkaria, J. N., & Elmquist, W. F. (2022). The influence of the blood–brain barrier in the treatment of brain tumours. *Journal of Internal Medicine*, *292*(1), 3–30.

Raval, N., Maheshwari, R., Kalyane, D., Youngren-Ortiz, S. R., Chougule, M. B., & Tekade, R. K. (2019). Importance of physicochemical characterization of nanoparticles in pharmaceutical product development. In *Basic fundamentals of drug delivery* (pp. 369–400). Elsevier.

Sánchez-Dengra, B., García-Montoya, E., González-Álvarez, I., Bermejo, M., & González-Álvarez, M. (2023). Establishment and validation of a new co-culture for the evaluation of the permeability through the blood–brain barrier in patients with glioblastoma. *Pharmaceutics*, *15*(5), 1431.

Saraiva, C., Praça, C., Ferreira, R., Santos, T., Ferreira, L., & Bernardino, L. (2016). Nanoparticle-mediated brain drug delivery: Overcoming blood–brain barrier to treat neurodegenerative diseases. *Journal of controlled release*, *235*, 34–47.

Schindelin, J., Arganda-Carreras, I., Frise, E., Kaynig, V., Longair, M., Pietzsch, T., Preibisch, S., Rueden, C., Saalfeld, S., Schmid, B., et al. (2012). Fiji: An open-source platform for biological-image analysis. *Nature methods*, *9*(7), 676–682.

Selim, M. M., El-Safty, S., Tounsi, A., & Shenashen, M. (2024). A review of magnetic nanoparticles used in nanomedicine. *APL Materials*, *12*(1).

Sharma, P., Aaroe, A., Liang, J., & Puduvalli, V. K. (2023). Tumor microenvironment in glioblastoma: Current and emerging concepts. *Neuro-Oncology Advances*, *5*(1), vdad009.

Skotland, T., Iversen, T.-G., & Sandvig, K. (2010). New metal-based nanoparticles for intravenous use: Requirements for clinical success with focus on medical imaging. *Nanomedicine: Nanotechnology, Biology and Medicine*, *6*(6), 730–737.

Sloan, E. A., Hilz, S., Gupta, R., Cadwell, C., Ramani, B., Hofmann, J., Kline, C. N., Banerjee, A., Reddy, A., Oberheim Bush, N. A., et al. (2020). Gliomas arising in the setting of li-fraumeni syndrome stratify into two molecular subgroups with divergent clinicopathologic features. *Acta neuropathologica*, *139*, 953–957.

Soto-Rojas, L. O., Pacheco-Herrero, M., Martínez-Gómez, P. A., Campa-Córdoba, B. B., Apátiga-Pérez, R., Villegas-Rojas, M. M., Harrington, C. R., de la Cruz, F., Garcés-Ramírez, L., & Luna-Muñoz, J. (2021). The neurovascular unit dysfunction in alzheimer's disease. *International journal of molecular sciences*, *22*, 1–27. https://doi.org/10.3390/IJMS22042022

Stueber, D. D., Villanova, J., Aponte, I., Xiao, Z., & Colvin, V. L. (2021). Magnetic nanoparticles in biology and medicine: Past, present, and future trends. *Pharmaceutics*, *13*(7), 943.

Stylianopoulos, T., Munn, L. L., & Jain, R. K. (2018). Reengineering the physical microenvironment of tumors to improve drug delivery and efficacy: From mathematical modeling to bench to bedside. *Trends in cancer*, *4*(4), 292–319.

Suk, J. S., Xu, Q., Kim, N., Hanes, J., & Ensign, L. M. (2016). Pegylation as a strategy for improving nanoparticle-based drug and gene delivery. *Advanced drug delivery reviews*, *99*, 28–51.

Tam, J. O., de Puig, H., Yen, C.-w., Bosch, I., Gómez-Márquez, J., Clavet, C., Hamad-Schifferli, K., & Gehrke, L. (2017). A comparison of nanoparticle-antibody conjugation strategies in sandwich immunoassays. *Journal of Immunoassay and Immunochemistry*, *38*(4), 355–377.

Thomsen, L. B., Burkhart, A., & Moos, T. (2015). A triple culture model of the blood-brain barrier using porcine brain endothelial cells, astrocytes and pericytes. *PloS one*, *10*(8), e0134765.

Thomsen, L. B., Linemann, T., Birkelund, S., Tarp, G. A., & Moos, T. (2019). Evaluation of targeted delivery to the brain using magnetic immunoliposomes and magnetic force. *Materials*, *12*(21), 3576.

Thomsen, L. B., Linemann, T., Pondman, K. M., Lichota, J., Kim, K. S., Pieters, R. J., Visser, G. M., & Moos, T. (2013). Uptake and transport of superparamagnetic iron oxide nanoparticles through human brain capillary endothelial cells. *ACS chemical neuroscience*, *4*(10), 1352–1360.

Thomsen, M. S., Humle, N., Hede, E., Moos, T., Burkhart, A., & Thomsen, L. B. (2021). The blood-brain barrier studied in vitro across species. *PLoS One*, *16*(3), e0236770.

Tripathy, D. K., Panda, L. P., Biswal, S., & Barhwal, K. (2024). Insights into the glioblastoma tumor microenvironment: Current and emerging therapeutic approaches. *Frontiers in Pharmacology*, *15*, 1355242.

Verkhratsky, A., & Nedergaard, M. (2018). Physiology of astroglia. *Physiological reviews*, *98*(1), 239–389.

Wilhelm, S., Tavares, A. J., Dai, Q., Ohta, S., Audet, J., Dvorak, H. F., & Chan, W. C. (2016). Analysis of nanoparticle delivery to tumours. *Nature reviews materials*, *1*(5), 1–12.

Wu, D., Chen, Q., Chen, X., Han, F., Chen, Z., & Wang, Y. (2023). The blood–brain barrier: Structure, regulation, and drug delivery. *Signal Transduction and Targeted Therapy*, *8*(1), 217.

Yallapu, M. M., Foy, S. P., Jain, T. K., & Labhasetwar, V. (2010). Peg-functionalized magnetic nanoparticles for drug delivery and magnetic resonance imaging applications. *Pharmaceutical research*, *27*, 2283–2295.

Ye, J., Coulouris, G., Zaretskaya, I., Cutcutache, I., Rozen, S., & Madden, T. L. (2012). Primer-blast: A tool to design target-specific primers for polymerase chain reaction. *BMC bioinformatics*, *13*, 1–11.

Yusuf, A., Almotairy, A. R. Z., Henidi, H., Alshehri, O. Y., & Aldughaim, M. S. (2023). Nanoparticles as drug delivery systems: A review of the implication of nanoparticles' physicochemical properties on responses in biological systems. *Polymers*, *15*(7), 1596.

Zhang, S., & Wang, C. (2023). Precise analysis of nanoparticle size distribution in tem image. *Methods and Protocols*, *6*(4), 63.

Zhao, M., Chang, J., Fu, X., Liang, C., Liang, S., Yan, R., & Li, A. (2012). Nano-sized cationic polymeric magnetic liposomes significantly improves drug delivery to the brain in rats. *Journal of drug targeting*, *20*(5), 416–421.

Zhao, X., Shang, T., Zhang, X., Ye, T., Wang, D., & Rei, L. (2016). Passage of magnetic tat-conjugated fe 3 o 4@ sio 2 nanoparticles across in vitro blood-brain barrier. *Nanoscale Research Letters*, *11*, 1–12.

Zheng, X., Ren, B., & Gao, Y. (2023). Tight junction proteins related to blood-brain barrier and their regulatory signaling pathways in ischemic stroke. *Biomedicine & Pharmacotherapy*, *165*, 115272.

Appendix A

A.1 TEER Values

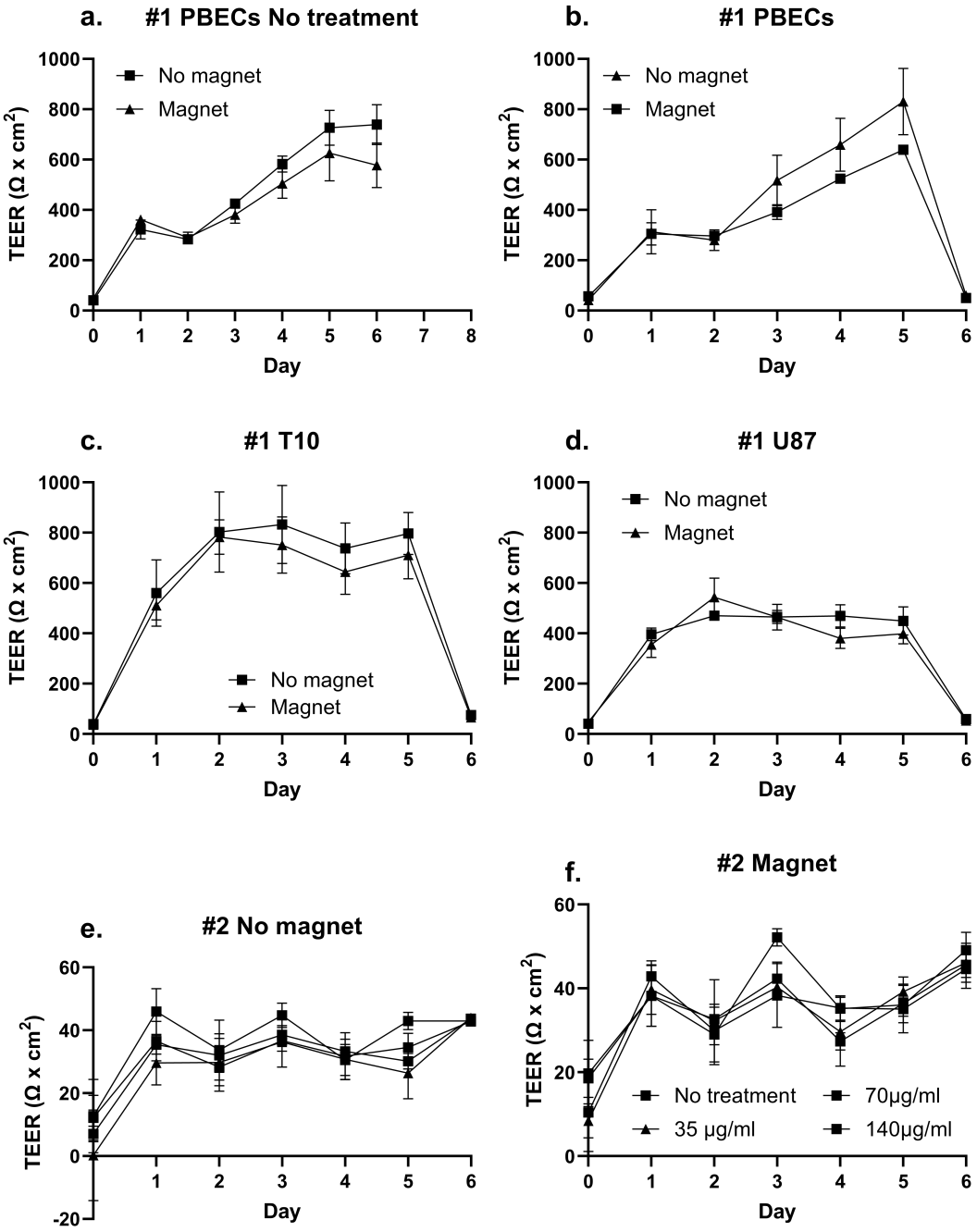

Figure A.1: TEER values for setup 1 and 2: TEER represented as mean±SD.

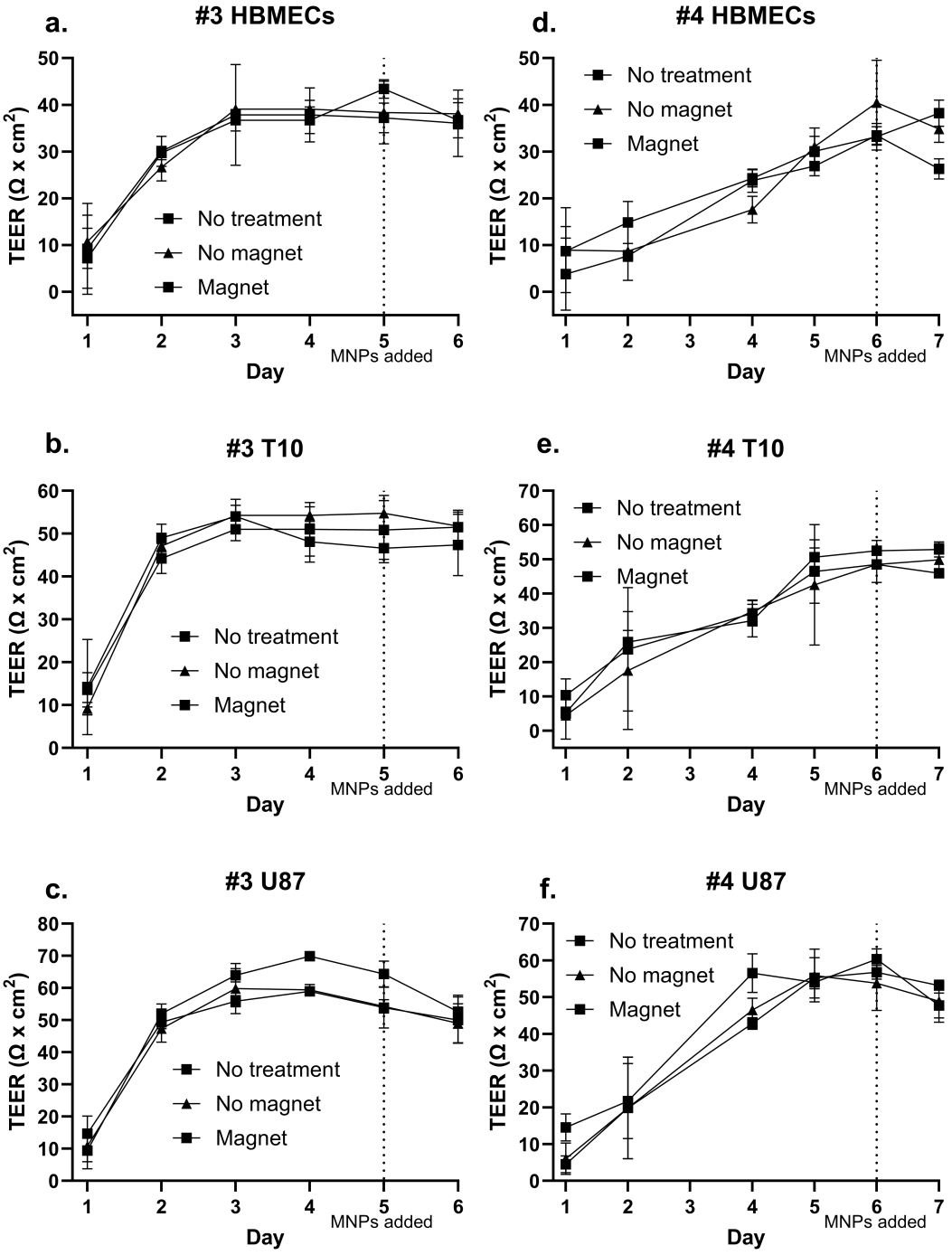

Figure A.2: TEER values for setup 3 and 4: TEER represented as mean±SD.